การเคลื่อนที่ภายในเซลล์ของอนุภาคออกซิไดซ์คาร์บอนระดับนาโนเมตรที่มีรูปทรงต่างกัน

นายบรรพต เจี้ยงเจริญ

วิทยานิพนธ์นี้เป็นส่วนหนึ่งของการศึกษาตามหลักสูตรปริญญาวิทยาศาสตรมหาบัณฑิต
สาขาวิชาเทคโนโลยีชีวภาพ
คณะวิทยาศาสตร์ จุฬาลงกรณ์มหาวิทยาลัย
ปีการศึกษา 2560

INTRACELLULAR TRAFFICKING OF DIFFERENT SHAPED OXIDIZED CARBON NANOPARTIC
LES

Mr. Banphot Jiangchareon

จุฬาลงกรณ์มหาวิทยาลัย
CHULALONGKORN UNIVERSITY

A Thesis Submitted in Partial Fulfillment of the Requirements

for the Degree of Master of Science Program in Biotechnology

Faculty of Science

Chulalongkorn University

Academic Year 2017

Thesis Title INTRACELLULAR TRAFFICKING OF DIFFERENT SHAPED OXIDIZED CARBON NANOPARTICLES

By Mr. Banphot Jiangchareon

Field of Study Biotechnology

Thesis Advisor Professor Supason Wanichwecharungruang, Ph.D.

Thesis Co-Advisor Associate Professor Tanapat Palaga, Ph.D.

Accepted by the Faculty of Science, Chulalongkorn University in Partial Fulfillment of the Requirements for the Master's Degree

---Dean of the Faculty of Science

(Professor Polkit Sangvanich, Ph.D.)

THESIS COMMITTEE

---Chairman

(Associate Professor Vudhichai Parasuk, Ph.D.)

---Thesis Advisor

(Professor Supason Wanichwecharungruang, Ph.D.)

---Thesis Co-Advisor

(Associate Professor Tanapat Palaga, Ph.D.)

---Examiner

(Associate Professor Preecha Phuwapraisirisan, Ph.D.)

---External Examiner

(Assistant Professor Thitinun Karpkird, Ph.D.)

บรรพต เจี้ยงเจริญ : การเคลื่อนที่ภายในเซลล์ของอนุภาคออกซิไดซ์คาร์บอนระดับนาโน เมตรที่มีรูปทรงต่างกัน (INTRACELLULAR TRAFFICKING OF DIFFERENT SHAPED OXIDIZED CARBON NANOPARTICLES) อ.ที่ปรึกษาวิทยานิพนธ์หลัก: ศ. ดร.ศุภศร วนิช เวชารุ่งเรือง, อ.ที่ปรึกษาวิทยานิพนธ์ร่วม: รศ. ดร.ธนาภัทร ปาลกะ, หน้า.

อนุภาคออกซิไดซ์คาร์บอนแบบกลม (OCSs) และแบบแผ่น (GOShs) ถูกเตรียมจากการ ออกซิเดชันแกรไฟต์ อนุภาคออกซิไดซ์คาร์บอนแบบแท่ง (OCTs) ถูกเตรียมจากการออกซิเดชัน อนุภาคคาร์บอนแบบแท่ง อนุภาคออกซิไดซ์คาร์บอนทั้ง 3 รูปทรงได้นำไปใช้ในการศึกษาเส้นทาง การเคลื่อนที่ภายในเซลล์ทั้ง 3 ชนิดได้แก่ human embryonic kidney cells (HEK293T), mouse macrophage cells (RAW264.7) และ human liver cancer cells (HepG2) จากการทดลอง อนุภาคออกซิไดซ์แบบทรงกลม แบบแท่ง และแบบแผ่น เข้าสู่เซลล์ HEK293T และ RAW264.7 โดย ไม่ผ่านกระบวนการ endocytosis และกระจายตัวอยู่ใน cytoplasm ในขณะเดียวกันอนุภาค ออกซิไดซ์คาร์บอนทั้ง 3 รูปทรงยังสามารถพบได้ใน lysosome ของเซลล์ HEK293T แต่ใน lysosome ของเซลล์ RAW264.7 พบแค่รูปทรงแบบแท่ง และแผ่นเท่านั้น อนุภาคออกซิไดซ์คาร์บอน แบบทรงกลมสามารถหลบเลี่ยงจากการถูกย่อยสลายใน lysosome ของเซลล์ RAW264.7 ใน เซลล์ HepG2 นั้นพบว่าอนุภาคออกซิไดซ์คาร์บอนทั้ง 3 รูปทรงเคลื่อนที่เข้าสู่เซลล์ผ่านกระบวานการ endocytosis อนุภาคออกซิไดซ์คาร์บอนทั้ง 3 รูปทรงถูกพบอยู่ใน endosome และ lysosome และยังพบอีกว่าการเคลื่อนที่ภายในเซลล์ของอนุภาคออกซิไดซ์คาร์บอนทั้ง 3 รูปทรง ในเซลล์ HEK293T และ HepG2 ถูกพบอยู่ในแค่ golgi apparatus และไม่ถูกพบใน endoplasmic reticulum (ER) แต่ในเซลล์ RAW264.7 อนุภาคออกซิไดซ์คาร์บอนทั้ง 3 รูปทรงเคลื่อนภายใน เซลล์ผ่าน ER และ golgi apparatus นอกจากนี้การเปรียบเทียบความต่างของรูปทรง พบว่า อนุภาคออกซิไดซ์คาร์บอนแบบทรงกลมสามารถเข้าสู่เซลล์ได้ไวที่สุด แบบแท่งเข้าสู่เซลล์ได้ ระดับกลาง และแบบแผ่นเข้าเซลล์ได้ช้าที่สุด จากผลที่กล่าวมามีแนวโน้มที่สามารถนำอนุภาค ออกซิไดซ์ประยุกต์ใช้ทางด้านชีวการแพทย์ และการนำส่งสาร โดยเฉพาะอนุภาคคาร์บอนแบบทรงกลม (OCSs) ที่สามารถเข้าเซลล์ได้ไวที่สุด และหลบเลี่ยงจากการถูกย่อยด้วย lysosome ในเซลล์ภูมิคุ้มกัน

สาขาวิชา	เทคโนโลยีชีวภาพ	ลายมือชื่อนิสิต	....
ปีการศึกษา	2560	ลายมือชื่อ อ.ที่ปรึกษาหลัก	....
		ลายมือชื่อ อ.ที่ปรึกษาร่วม	....

5772034223 : MAJOR BIOTECHNOLOGY

KEYWORDS: INTRACELLULAT TRAFFICKING / OXIDIZEDC CARBON NANOSPHERES / OXIDIZED CARBONANOTUBES / GRAPHENE OXIDE SHEETS

BANPHOT JIANGCHAREON: INTRACELLULAR TRAFFICKING OF DIFFERENT SHAPED OXIDIZED CARBON NANOPARTICLES. ADVISOR: PROF. SUPASON WANICHWECHARUNGRUANG, Ph.D., CO-ADVISOR: ASSOC. PROF. TANAPAT PALAGA, Ph.D., pp.

Oxidized carbon nanospheres (OCSs) and graphene oxide sheets (GOShs) were prepared by oxidation of graphite. Oxidized carbon nanotubes (OCTs) was synthesized from single-walled carbon nanotubes. All three shapes of oxidized carbon nanoparticles (OCNs) were used for investigation of their intracellular trafficking in human embryonic kidney cells (HEK293T), mouse macrophage cells (RAW264.7) and human liver cancer cells (HepG2). The results revealed all three shapes of OCNs were internalized into through HEK293T and RAW264.7 cells without endosomal trapping, including localization of all the three OCNs in HEK293T's lysosome. In case of RAW264.7 cells, OCTs and GOShs were localized in lysosomes, only OCSs can escape from degradation in RAW264.7's lysosome. In case of HepG2 cells, the three shapes of OCNs were internalized into the cells through endocytosis, OCSs, OCTs and GOShs were localized in endosome and lysosome. Furthermore, the all three shapes of OCNs were found in golgi apparatus in HEK293T and HepG2 cells. In case of RAW264.7 cells, OCSs, OCTs and GOShs were localized in endoplasmic reticulum and golgi apparatus. In addition, comparison of different shaped OCNs revealed that OCSs was the fastest cellular internalization, OCTs was moderate and GOShs was the slowest cellular internalization. Hence, oxidized carbon nanoparticles had great potential be applied in biological and biomedical applications, including drug delivery system. Especially, OCSs was capable of the fastest cellular internalization and evasion of lysosomal degradation.

Field of Study: Biotechnology   Student's Signature ....

Academic Year: 2017   Advisor's Signature ....

                                     Co-Advisor's Signature ....

ACKNOWLEDGEMENTS

Firstly, I would like to express my sincere gratitude to my advisor Prof. Dr. Supason Wanichwecharungruang for the continuous support of My Master degree study and related research, for her patience, motivation, and immense knowledge. Her guidance helped me in all the time of research and writing of this thesis.

I would like to grateful acknowledge to my co-advisor, Assoc. Prof. Dr. Tanpat Palaga for his contributions of time, immense knowledge, and experience in the biological parts.

I am sincerely grateful to the members of the thesis committee, Asst. Prof. Dr. Varawut Tangpasuthadol, Assoc. Prof. Dr. Preecha Phuwapraisirisan, Assist Prof. Dr. Thitinun Karpkird for their valuable comments and suggestions.

I am profoundly grateful Dr. Trairak Pisitkun, Mr. Vitavat Aksornkitti and Chulalongkorn Academic Advancement into 2nd Century (CUAASC) project for their assistance and supported me in observing cellular images by using ZEISS LSM800 confocal laser scanning fluorescent microscope.

I would like to acknowledge the past and present members of SW research group om fourteen floor, Mahamakut building, TP research group twenty floor, Maha Vachirunahit building for their companionships and friendships And I would like to thank some special lovely friend, Ekkaphon Rattanagkool, Vasin Thummasorn, and Chanoknan Boonyaratsewee, for their assistance and friendship.

Nobody has been more important to me in the pursuit of this goal of my life than the members of my family. I would like to take this opportunity to express my sincere appreciation to my parents for their encouragement and support throughout the entire research study. This accomplishment would not have been possible without them.

CONTENTS

LIST OF FIGURES

LIST OF TABLES

LIST OF ABBREVTATIONS

λ_{em}	Emission wavelength
λ_{ex}	Excitation wavelength
GFP	Green fluorescent proteins
g	Gram
GOShs	Graphene oxide sheets
h	Hour
IgG	Immunoglobulin G
kV	Kilovolts
MHC	Major Histocompatibility complex
μL	Microliter
μm	Micrometer
μM	Micromolar
mg	Milligram
mL	Milliliter
min	Minute
nm	Nanometer
nM	Nanomolar
OCNs	Oxidized carbon nanoparticles
OCSs	Oxidized carbon nanospheres
OCTs	Oxidized carbon nanotubes
PBS	Phosphate buffer saline
v/v	Volume by volume
w/v	Weight by volume

CHAPTER I

INTRODUCTION

1.1 Introduction

Transductions of external cellular signals, such as hormones, neurotransmitters, and growth factors, occur on cell surface. In this process, receptors on the cell membrane is used for binding and transducing external signals inside of the cells. This process is vital for the whole cell function, tissues and organs. The disordered intra-cellular transport of signals result in aberrant cell growth, collapsing of cell functions and causing of human disease, for example, diabetes [1, 2], immunity disorder [3], cancer [4], heart diseases [5] and brain diseases [6]. Accordingly, intracellular trafficking need to be coordinated with other cellular signaling to allow cell growth [7], proper cellular signaling [8] and development if mutli-celllular organisms.

Carbon-based nanomaterials have versatile properties, are useful for drug delivery system, for example, various morphologies, large surface area, water dispersibility, easy surface modification, good stability and good biocompatibility [9-13]. In recent years, carbon-based nanomaterials are used as a carrier for sending substances, such as hydrophilic and hydrophobic compound [14-16], proteins [17-19], DNA/RNA [20-22] and nucleic acid [23], internalize to inside of the cells and enhance cellular process. Uptaken carbon-based nanomaterials are transported through intracellular trafficking pathway which, has two major pathway: endocytic pathway, internalizes substances from surroundings to inside of the cells [24]. exocytic pathway, secretes substances from cell cytoplasm to surroundings [2].

Organelles are in the cells, always coordinate with intracellular trafficking pathway, for instances, the substances are internalized through endocytic pathway, are wrapped by the cell membrane and contained into vesicles as endosomes [25]. In this pathway, endosomes transport the substances to lysosomes for degradation [26-28]. In addition, external-cellular signals are secreted to cell milieu through exocytic pathway. Exocytic compartments, such as endoplasmic reticulum and golgi apparatus

are required in this process [29-31]. Therefore, uptaken carbon-based nanomaterials and substances have possibility, facing many organelles in different pathways.

To understand intracellular trafficking of carbon-based nanomaterials. In this research, oxidized carbon nanospheres (OCSs), oxidized carbon nanotubes (OCTs) and graphene oxide sheets (GOShs), are represented three morphologies of carbon-based nanomaterials. Intracellular trafficking was studied through observation of colocalization between uptaken carbon-based nanomaterials and organelles inside of the cells, by using confocal laser scanning fluorescence microscope (CLSFM).

1.2 Literature review

1.2.1 Intracellular trafficking
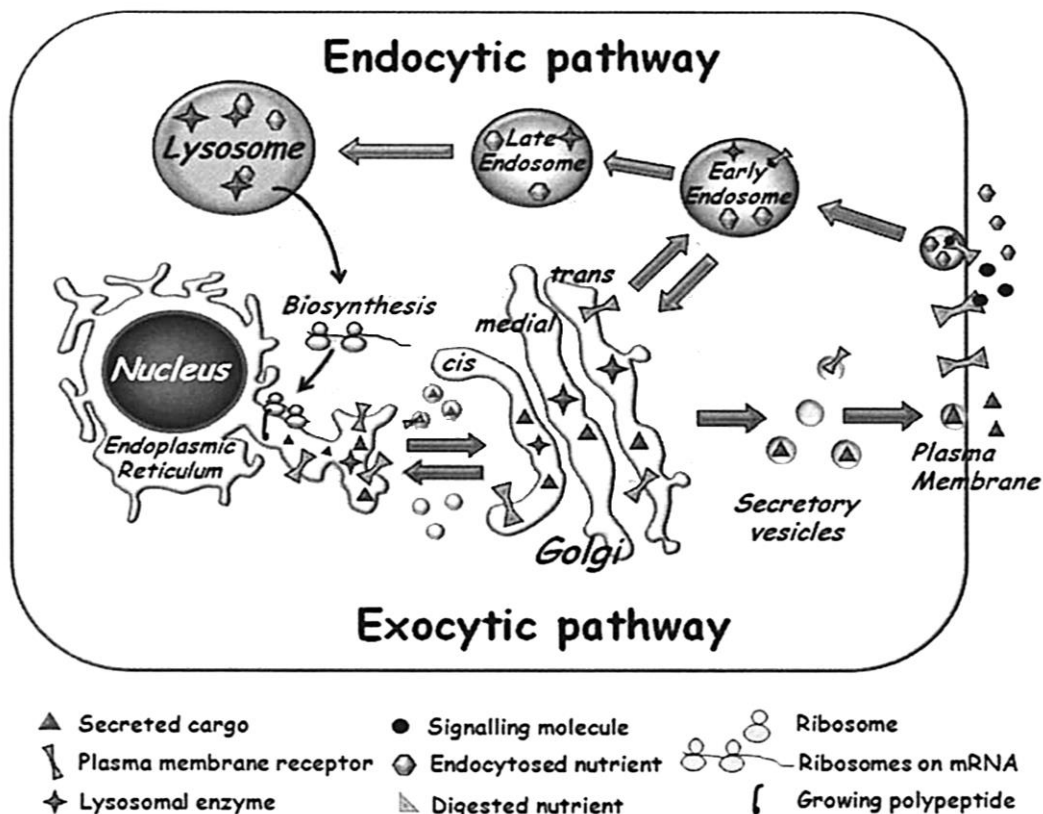
Figure 1.1: Schematic illustration of two major intracellular trafficking pathways and connection between substances and compartments [2, 24].

Cell membranes are a barrier for protecting and separating inside of the cells from their environments. The cells also have organelle membrane that compartmentalize and carry out specific cellular functions, such as nucleus for DNA replication and mitochondria for respiration. The compartmentalization in the cells increases efficiency of many subcellular by concentrating of required components in confined space within the cells. However, the compartmentalization lead to problem at the same time, that is the requiring for communication between different cellular compartments. Thus, the processing communication between another compartments is vesicle transport, which contained signaling proteins and transported to appropriate compartment and appropriated trafficking pathway. Typically, the cells have two major

trafficking pathway, that transport substances outward and inward, are used for connection of their compartment; exocytic pathway is route for secretion of signaling protein or cell products to outside of the cells and endocytic is route for internalization of extracellular proteins [32].

1.2.1.1 Exocytic pathway

In exocytic pathway, substances or proteins synthesized in cell cytoplasm are translocated into endoplasmic reticulum (ER) which is site of synthesis of proteins which involve with intercellular communication and connection of compartment by vesicular transport. From the ER, the cargos are shuttled through golgi apparatus for packing cargos into secretory vesicles or presentation on the cell membranes (**Figure 1.1**) [2].
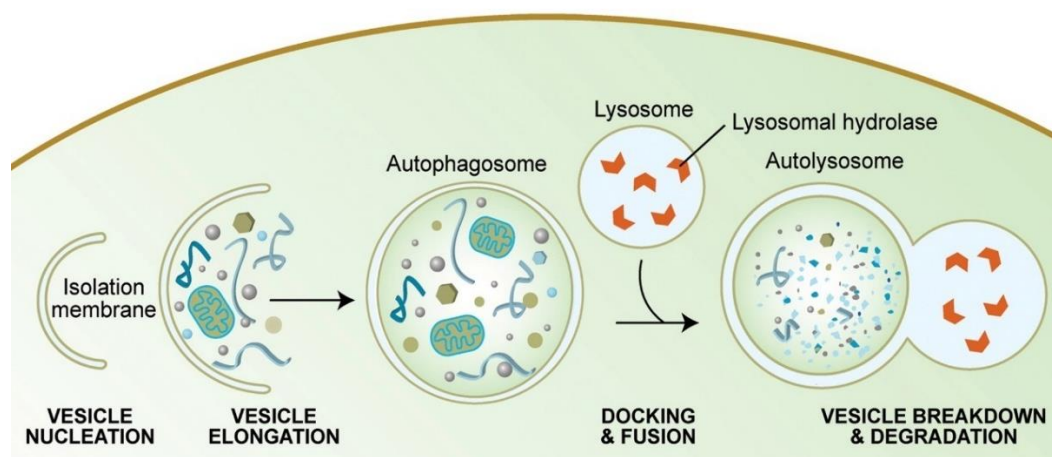
Figure 1.2: Schematic illustration of autophagic pathaway [33].

1.2.1.2 Endocytic pathway

In endocytic pathway, proteins or substances are internalized from the cell environments *via* endocytosis, which is formed by membrane to become as the endosomes for intracellular transportation. The route of endosomes is shuttling cargos to lysosomes, which is site of degradation. In lysosomes, they contain hydrolytic enzymes to degrade internalized substances (**Figure 1.1**). In addition, cellular protein in cell cytoplasm can to lysosomes through autophagy, which the cells create lipid-

layer membrane inside of them and engulf cellular protein for transportation to lysosomes and translocate to outside of the cells (**Figure 1.2**) [24, 33, 34].

1.2.2 Carbon-based nanomaterials

Recently, several researches are reported that carbon-based nanomaterials are potentially applied in biological and biomedical applications, including their versatile property such as, biocompatibility, low cytotoxicity and high surface areas. Cause of their properties, carbon-based materials are used as vehicles for delivery active compound into the cells and protecting enzymatic cleavage [9, 11, 35, 36].

1.2.2.1 Carbon nanotubes

Carbon nanotubes are conceived as a rolled-sheet of graphite, which has been shaped into a tube. Carbon nanotube are consisted of linked sp^2-carbon as network, so that surface of carbon nanotubes has hydrophobic property. Generally, carbon nanotubes are not water-dispersible, their surfaces are modified for increasing water-dispersibility. There are properties of carbon nanotubes, are widely used a carrier, for example, bio-compatibility, low-cytotoxicity, and high surface area, that for adsorbing many active molecules. Hence, their applications are used for delivery of therapeutically active molecules to target cells [37-41].
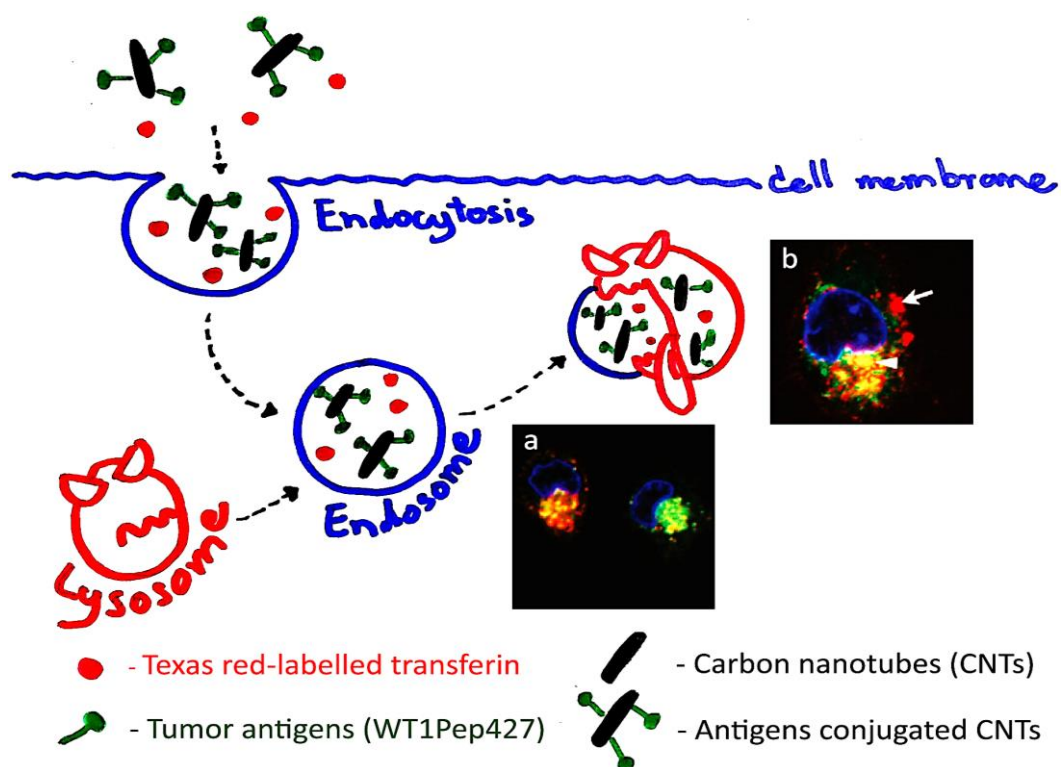
Figure 1.3: Schematic endocytosis of tumor antigens-conjugated with SWNCT in dendritic cells (DCs). Image (a) shows co-staining of WT1Pep427 conjugated SWCNTs-FITC (green) and Texas red-labelled transferrin (red). Image (b) shows co-localization of lysosomes (red) and FITC conjugated with SWCNTs (green) as a punctate yellow vesicles (arrowhead) [18, 24].

In 2011, Carlos *et al*. used single-walled carbon nanotubes (SWCNTs), conjugated with WT1 peptide 427 (WT1Pep427) as a tumor antigen model, to enhance immune response in dendritic cells (DCs) (**Figure1.3**). WT1Pep427-conjugated with SWCNTs were uptaken in to the cells by endocytosis pathway. This process generated IgG response by MHC class II molecules in endocytosis compartment [42]. In addition, WT1Pep427-conjuagted with SWCNTs and Titermax, as an adjuvant, were simultaneously immunized in mice, result in IgG serums, that specifically responded to WT1Pep427, were produced [18].
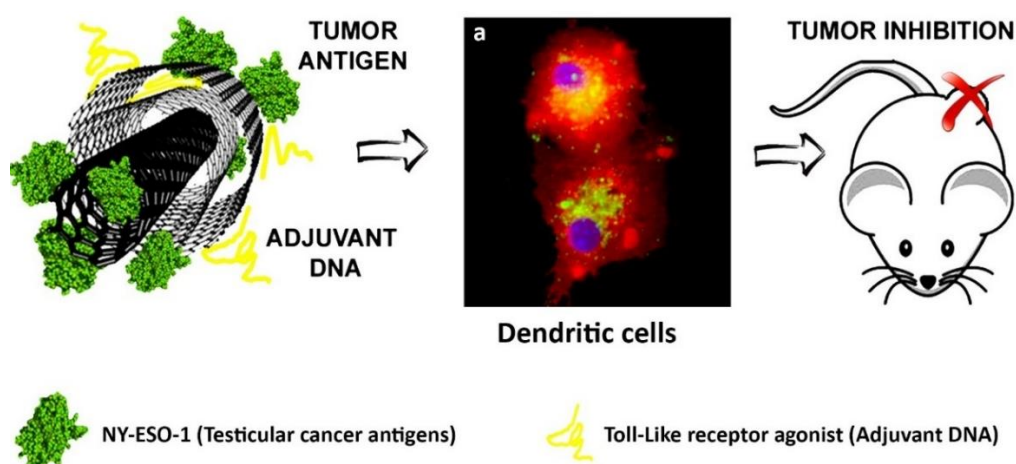
Figure 1.4: Schematic illustration of oxidized multi-walled carbon nanotubes (MWCNTs) as an antigen delivery to induce immune response in dendritic cells. (a) Confocal fluorescent image showed MWCNTs (green) in cytoplasm (red), were mainly distributed in perinuclear region of dendritc cells [43].

In 2014, Paula *et al.* immobilized testicular cancer antigen (NY-ESO-1) and Toll-Like receptor (TLR) agonist on surface of oxidized multi-walled carbon nanotubes (MWCNTs) (**Figure 1.4**). Oxidized MWCNTs were used for sending tumor antigen and TLR agonist and promoting immune response in dendritic cells (DCs). Oxidized MWCNTs were phagocyted and distributed in cell cytoplasm of DCs. In addition, internalized oxidized MWCNTs localized in perinuclear region of DCs [43].
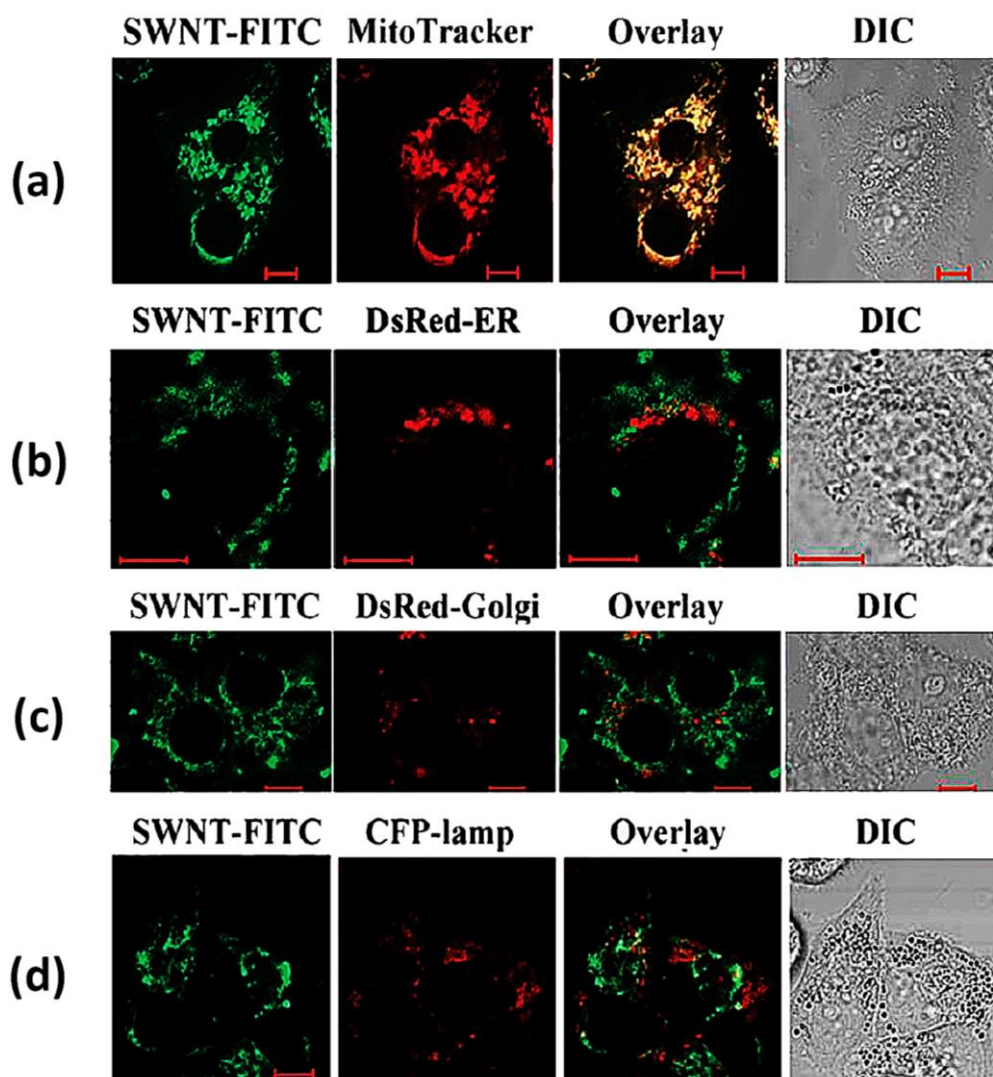
Figure 1.5: Confocal microscopy images of SWNCTs-PL-PEG in subcellular compartment (red) of Hela cells. (a) mitochondria, (b) endoplasmic reticulum, (c) golgi apparatus, (d) lysosome. (left to right) SWCNTs-PL-PEG-FITC (green), subcellular compartments were labelled with dye (red), merged fluorescence images and DIC images [44].

In 2010, Feifan *et al*. confirmed subcellular localization of single-walled carbon nanotubes (SWCNTs) in Hela cells; SWCNTs were modified by conjugation with phospholipid-polyethylene glycol (PL-PEG) leading to improvement of water-dispersibility. SWCNT-PL-PEG was labelled with fluorescein isothiocyanate (FITC) for imaging subcellular localization under confocal laser scanning fluorescent microscope

(**Figure 1.5**). SWCNTs-PL-PEG-FITC showed internalization into the cells, without active transport, and localized in mitochondria, not any other subcellular compartment in Hela cells. In addition, subcellular localization of SWCNTs-PL-PEG-FITC was determined the cell line dependence in different cells (ASTC-a-1, MCF7, COS7, EVC304, and RAW264.7), which tumor cells or normal cells showed localization in mitochondria. Furthermore, SWCNTs-PL-PEG-FITC was localized in lysosomes in macrophage cell line [44, 45].

1.2.2.2 Graphene oxide sheets

Typically, basal structure of graphite contained network of sp^2-carbon atom, was hydrophobic and not dispersible in water. Graphene oxide sheets (GOShs) was products of oxidation graphite under acid condition, can disperse in water. The structure of GOShs was composed of graphene planes, that was hydrophobic, with polarized functional groups, such as, carboxylate, hydroxyl (-OH), and epoxide (-O-). Hence, GOShs had capability of $\pi-\pi$ interaction from graphene relevant to adsorbing of dye or active molecules, and colloidal stability in water [46, 47].

จุฬาลงกรณ์มหาวิทยาลัย
CHULALONGKORN UNIVERSITY

inhibitor	affected mechanism	target
colchicine	mitosis	tubulin: microtubule polymerization alteration and cell cycle arrest in metaphase.
wortmannin	phagocytosis	PI3K (selective) and other kinases as miosine light chain kinase and PI4K.
amiloride	macropinocytosis	Na$^+$/H$^+$ exchanger. Unspecific.
cytochalasin B	macropinocytosis	actin: blockage of its polymerization avoiding microfilaments action.
cytochalasin D	macropinocytosis	actin: blockage of its polymerization avoiding microfilaments action and inhibition of other endocytosis routes.
genistein	clathrin-independent endocytosis	caveolae: inhibition of Src tyrosine kinases and caveolae dynamics.
phenylarsine oxide (PAO)	clathrin-dependent endocytosis	tyrosine phosphatases: membrane fluidity decrease and thiol groups oxidation.
chlorpromazine	clathrin-dependent endocytosis	clathrin: alteration of clathrin-coat assembly, membrane fluidity and permeability.

Figure 1.6: Histograms of %FITC incorporation represented effects of specific endocytosis inhibitors on FITC-PEG-GOs in Soas-2, HepG2 and RAW264.7 cells [48].

In 2014, Javier *et al.* determined endocytosis mechanism of PEGylated oxidized graphene sheets (PEG-GOs) PEG-GOs was labelled with fluorescein isothiocynate (FITC-PEG-GOs), and evaluated in presence of endocytosis inhibitor with different cells (osteoblasts (Saos-2), hepatocytes (HepG2), and macrophage (RAW264.7)) (**Figure 1.6**). FITC-PEG-GOs revealed internalization in to the cells through micropinocytosis in Saos-2, as a general mechanism. Moreover, HepG2 and RAW264.7 uptaken FITC-PEG-GOs through clarthin-dependent endocytosis. HepG2 also phagocytized FITC-PEG-GOs [48].
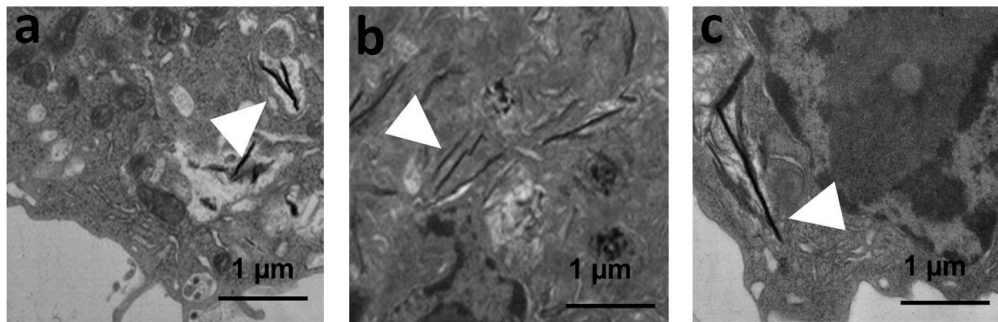
Figure 1.7: Transmission electron microscopy (TEM) images of dendritic cells (DCs). DCs were incubated with ovalbumin (OVA)-adsorbed graphene oxide nanosheets (GO-nS). (a) zoomed image displayed GO-nS inside a vesicle, (b) zoomed image displayed outside a vesicle, (c) zoomed image displayed piercing through the vesicle membrane. White arrows indicate the events of interest [24, 36].

In 2016, Hui *et al.* used graphene oxide nanosheets (GOx) for delivery vaccine protein. Ovalbumin (OVA) was used as models of vaccine antigen, and spontaneously adsorbed by GOx without requirement of any additional linker strategy (GOx:OVA). Both of GOx and GOx:OVA showed internalization into dendritic cells (DCs) under imaging by CLSFM. Transmission electron microscopy (TEM) revealed that GOx was found inside vesicles, which can be endosome or phagosome. In addition, GOx still be found outside the vesicles because its pierce through vesicle membranes (**Figure 1.7**) [36].
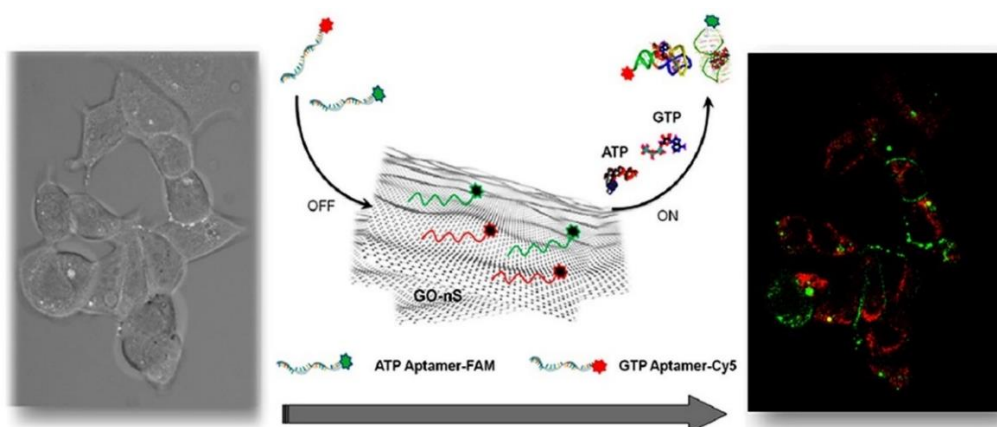
Figure 1.8: Schematic illustration of Graphene oxide nanosheet (GO-nS) as a ATP sensing in breast cancer cells (MCF7) [20].

In 2013, Ying *et al*. applied graphene oxide nanosheets (GO-nS) with DNA/RNA aptamer for measuring cellular ATP-level in living cells. DNA/RNA aptamer were derivative of adenosine or guanosine, were capable of ATP sensing. GO-nS was used for adsorption of fluorescent dye-labelled DNA/RNA aptamers on its surface (Aptamer/GO-nS) and monitored fluorescent property of aptamer in breast cancer cells (MCF7) under CLSFM (**Figure 1.8**). Aptamer/GO-nS showed internalization into the cells and monitoring ATP-level. In addition, GO-nS demonstrated good-biocompatibility to living cells and protecting of enzyme digestion [20].

1.2.2.3 Carbon nanospheres

Carbon nanospheres were visualized as spherically self-assembly of graphene sheets, which their diameter was around 100-200 nm. Surface of carbon nanospheres consisted of hydrophobic planes of graphene sheets and high polar functional groups, for examples, carboxylate, hydroxyl (-OH), and epoxide (-O-). Hence, carbon nanospheres resulted in spherical amphiphilic particles. Carbon nanospheres performed as vehicles that deliver active molecules into target cells[15, 16, 23].
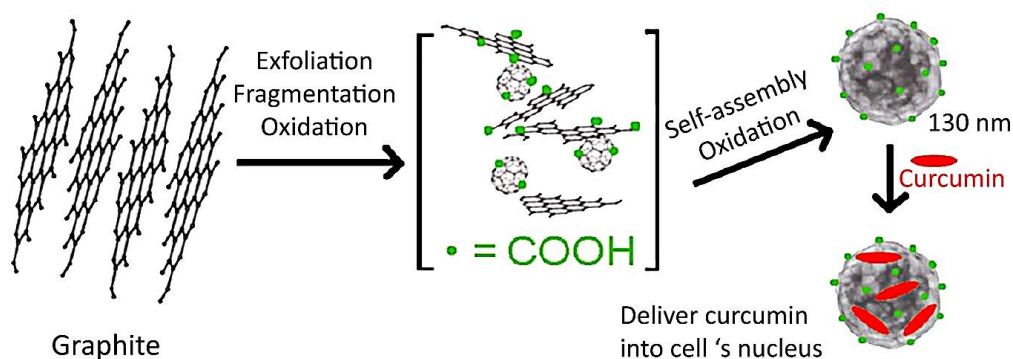
Figure 1.9: Synthesis cluster of carbon nanospheres [16].

In 2012, Sunatda *et al.* synthesized clusters of carbon nanospheres (CCN) through oxidation of graphite (**Figure 1.9**), which provided polar functional groups on surfaces of CCN such as, carboxylate and hydroxyl, likewise CCN afforded stabilized suspending in water. CCN were assessed cytotoxicity in HEK293T and CaSki cell lines, which concentration of CCN at 0.01 up to 10 µg/ml had no cytotoxicity. Hence, CCN were used for delivery of curcumin into HEK293T cells which cellular localization of CCNs was in cytoplasm of HEK293T cells and not in nucleus. Furthermore, loaded curcumin by CCN remained localized in the nucleus [16].
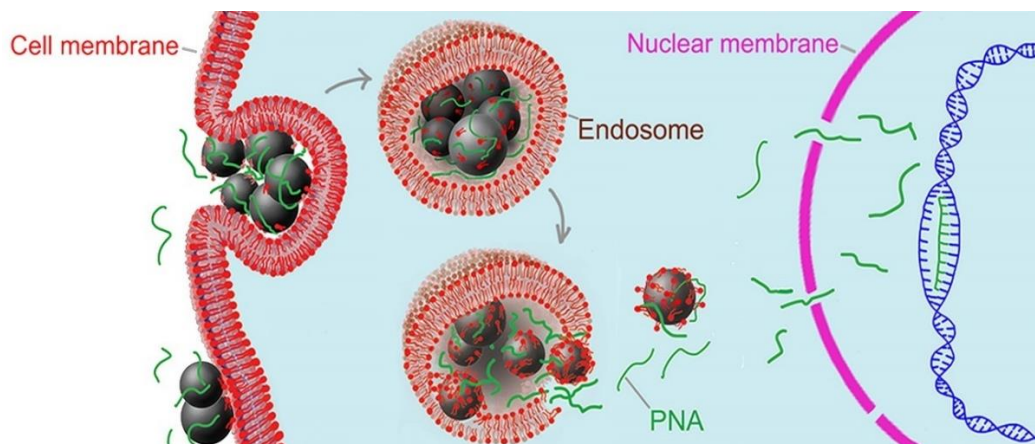
Figure 1.10: Schematic illustration of PNA delivery by using membrane penetrating oxidized carbon nanoparticles as a vehicles [23].

In 2015, Sunatda *et al*. demonstrated delivered acpcPNAs, which were peptide-nucleic acids (PNAs), by using of membrane penetrating oxidized carbon nanoparticles (MPOCs) as vehicles into RAW264.7 cells (**Figure 1.10**). acpcPNAs were demonstrated potential binding affinity and specificity complementary genes or DNAs, that suppressing *IL6* gene transcription. Delivered acpcPNAs by MPOCs resulted inhibition of *IL6* expression in RAW264.7. Delivered acpcPNAs with MPOCs, were entrapped by endosome in early state of incubation and immigrated to cytoplasm in late state of incubation. In addition, cellular uptake of acpcPNAs and MPOCs did not localize with lysosomes [23, 49].
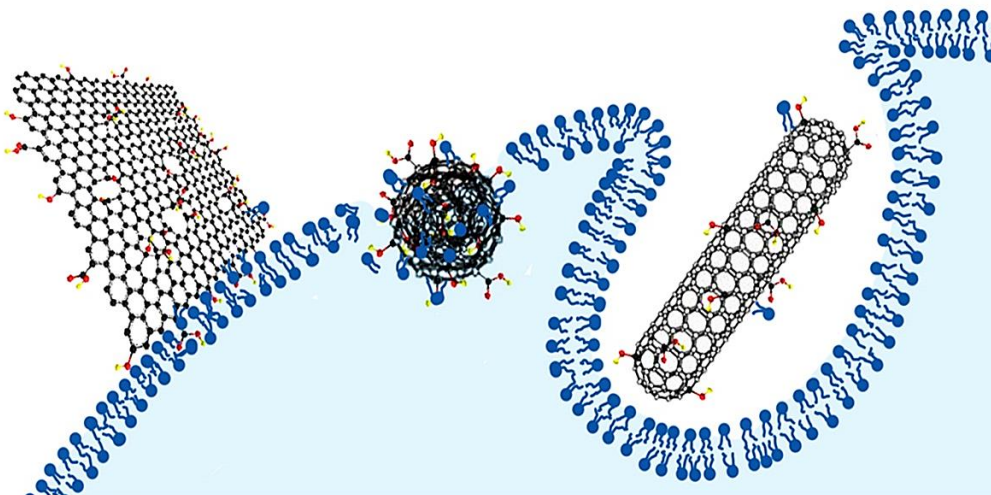
Figure 1.11: Schematic comparison of membrane-bound association between graphene oxide sheets (GOShs), oxidized carbon nanotubes (OCTs) and oxidized carbon nanospheres (OCSs) [15].

In 2016, Jiraporn *et al.* compared cellular uptake of curcumin, which was loaded into oxidized carbon nanospheres (OCSs) with oxidized carbon nanotubes (OCTs) and graphene oxide (GOShs) in A549 lung cancer cells. Cellular uptake of curcumin level by OCSs were higher than OCTs and GOShs, respectively. OCSs led curcumin nucleus of the cells, whereas OCTs only led curcumin to cytoplasm. GOShs revealed slightly cellular uptake of curcumin level and curcumin did not localize with nucleus. Additionally, Intracellular trafficking in HEK293T cells were also compared with fluorescein-labelled OCSs, OCTs and GOShs. HEK293T cells phagocytized OCTs and GOShs, which entrapped in lysosomes. Whereas, OCSs were uptaken without endosomal trapping and localized in cytoplasmic compartment [15].

1.3 Research objectives

Recently, there were various shapes of carbon-based materials which their applications were used for delivery active compound into the cells. However, distinguishing cellular uptake and intracellular trafficking pathway of various shapes of carbon-based materials were not reported, clearly. Hence, we synthesized three shapes of oxidized carbon nanoparticles were prepared into sheet, tubular and spherical shapes, that were used for representation of carbon-based nanomaterials. Three shapes of oxidized carbon-based materials were studied with their intracellular trafficking and cellular compartment localization.

CHAPTER II

EXPERIMENTAL

2.1 Synthesis and characterization of oxidized carbon nanoparticles

In this work, we synthesized three shapes of oxidized carbon nanoparticles, oxidized carbon nanospheres (OCSs), oxidize graphene sheets (GOShs) and oxidized carbon nanotubes (OCTs).

2.1.1 Preparation of oxidized carbon nanospheres (OCSs) and oxidized graphene sheets (GOShs)

OCSs and GOShs were prepared by oxidation of graphite. Graphite powder (1 g, Thai Carbon and Graphite Co., Ltd., Bangkok, Thailand) and sodium nitrate (1 g, Suksapan, Bangkok, Thailand) were mixed together and dispersed in 50 mL of 18 M sulfuric acid (Merck, Darmstadt, Germany). The mixture was sonicated at 40 kHz at room temperature for 1 h. Then, $KMnO_4$ (6 g, Sukasapan, Bangkok, Thailand) was added slowly and stirred for 90 min. Then, 100 mL of water were added and temperature maintained at 90 $^\circ$C for 30 min. After that, 300 mL of water was added. The mixture was stirred for 10 min. Next, excess $KMnO_4$ was eliminated by adding 5% H_2O_2 (50 mL, Merck, Darmstadt, Germany) and stirred continuouslty at room temperature for 30 min. The mixture was dialyzed against water to reduce acidity by dialysis membrane (CelluSup T4, MWCO of 12-14 kDa, Membrane Filtration Products, USA). When the pH value of dialysate was around 5-6. Product was separated by multi-step gradient centrifugation. First, the suspension was centrifuged at 9400 g for 10 min to precipitate large sized carbon debris, followed by centrifugation of supernatant at 11300 g for 15 min to precipitate small-sized debris. Next, GOShs was precipitated by centrifugation at 21100 g for 15 min. Finally, the supernatant was centrifuged at 37000 g for 30 min to remove the smaller GOShs and some debris. In this step, OCSs was found in supernatant.

2.1.2 Preparation of oxidized carbon nanotubes (OCTs)

Single- walled carbon nanotubes (SWCNTs, TCI, Tokyo, Japan) is starting materials for the preparation of OCTs. The oxidation of SWCNTs is similar to oxidation of OCSs and GOShs. Briefly, 1 g of SWCNTs and 1 g of sodium nitrate were mixed together. The mixture was added 50 ml of 18 M of H_2SO_4 and stirred for 10 min. Then, the mixture was added 6 g of $KMnO_4$ and stirred continuously for 30 min. Next, excess $KMnO_4$ was removed by adding 50 mL of 5% H_2O_2 and stirred for 10 min. The mixture was adjusted pH by dialysis against with water. Finally, the mixture was removed carbon debris by centrifugation at 11300 g for 15 min. The supernatant contained OCTs.

2.1.3 Characterization of oxidized carbon nanospheres (OCSs), oxidized carbon nanotubes (OCTs) and oxidized graphene sheets (GOShs)

For functional groups characterization, the obtained OCSs, OCTs, and GOShs were subjected to attenuated total reflectance fourier transform infared spectrometry (ATR-FTIR, Nicolet 6700, Thermo Electron Corporation, Waltham, Massachusetts, USA) and collected infared spectrum. In addition, all Raman spectra were collected by DXR™ Raman Microscope (Thermo Scientific, Thermo Fisher Scientific Inc., MA, USA). Morphology was determined by scanning electron microscopy (SEM, JSM-6400, JOEL, Tokyo, Japan; the samples were coated with gold under vacuum at 15 kV for 90s and observed at an accelerating voltage of 15 kV) and transmission electron microscopy (TEM, JEM-2100, JOEL, Tokyo, Japan; operated at 100-120 kV). Hydrodynamic diameter was obtained from Zetasizer (Nanoseries model S4700, Malvern Instruments, Worcestershire, UK).

2.2 Fluorescent dye labelling of oxidized carbon nanoparticles

To observe intracellular trafficking of oxidized carbon nanoparticles, OCSs, OCTs and GOShs, were labelled with two types of fluorescent dye. 5(6)-Carboxytetramethylrhodamine (TAMRA, Sigma-Aldrich, Missouri, USA) and 5-carboxyfluorescein (Sigma-Aldrich, Missouri, USA), EDCI/NHS coupling reaction was used to change carboxylic group of fluorescent dyes to succinimidyl ester and react with hydroxyl group of oxidized carbon nanopartcles. First, 25 μL of fluorescent dye solution (6.5 mg of TAMRA or 5.4 mg of 5-carboxyfluorescein in 500 μL DMF) was slowly added to 25 μL of EDCI solution (7.8 mg of EDCI in 500 μL DMF) and stirred for 30 min at 0 $^{\circ}$C, under N2 atmosphere. After that, 25 μL of NHS solution (4 mg of NHS in 500 μL DMF) was added to the mixture and stirred for 10 min. Lastly, aqueous suspension of OCSs, OCTs and GOShs (500 μg/mL, 5 mL) was added to mixture and stirred for overnight. All products were purified by dialysis (Dialysis cellulose membrane, MWCO = 12-14 kDa, Sigma Aldrich, St. Louis, USA). The products were monitored for their fluorescence property by using confocal laser scanning fluorescent microscope.

2.3 HEK293T cell lines

Human embryonic kidney cell lines (HEK293T, ATCC CRL-3216) were cultured in Dulbecco's modified eagle's medium (DMEM) supplemented with 10% (v/v) fetal bovine serum (FBS), 1% (w/v) sodium pyruvate, 1% (w/v) N-2-hydroxy-ethylpiperazine-N'-2-ethanesulfonic acid (HEPES), 1% (w/v) penicillin/streptomycin (all reagents were purchased from HyClone, Utah, USA) at 37 ^{0}C in humidified atmosphere of 5% (v/v) CO_2 incubator (Thermo Electron Corporation, USA).

2.3.1 Cell preservation

HEK293T cells were resuspended in 1 mL freezing media (10% (v/v) DMSO (Sigma-Aldrich, USA) in DMEM complete medium) and transferred to cryovial (SPL, Life sciences, Korea). Cells were stored at -80°C.

2.3.2 Cell preparation

HEK293T cells were collected by using 0.25% (w/v) trypsin/EDTA solution from container (T25 flask, Nunc, Thermo Fisher Scientific, UK) and centrifuged at 1000 rpm for 5 mins. Cell pellets were resuspended in DMEM complete medium and stained by 0.4% (w/v) tryphan blue stain (Gibco, USA). Cells were counted by hemacytometer. The number of viable cell was calculated using the following formula:

$$\text{The number of cells} = \frac{\text{(number of counted cells in 16 large square)}}{4} \times \text{dilute factor} \times 10^4$$

2.4 RAW264.7 cell lines

Mouse macrophage cell lines (RAW264.7, ATCC TIB-71) were cultured in DMEM medium, containing 10% (v/v) FBS, 1% (w/v) HEPES free acid, 1% (w/v) sodium pyruvate and 1% (w/v) penicillin/streptomycin at 37 ^{0}C in humidified atmosphere of 5% (v/v) CO_2 incubator.

2.4.1 Cell preservation

RAW264.7 cells were resuspended in 1 mL freezing media (10% (v/v) DMSO in DMEM complete medium) and transferred to cryovial. Cells were stored at -80 $^\circ$C.

2.4.2 Cell preparation

RAW264.7 cells were collected from sterile petri dishes (Biomed, Thailand) using PBS and centrifuged at 1000 rpm for 5 mins. Cell pellets were resuspended in DMEM complete media and stained by 0.4% solution of trypan blue stain. Cells were counted by hemacytometer. Cell were counted and calculated as showed in previous section.

2.5 HepG2 cell lines

Human hepatocellular carcinoma (HepG2, generous gifts from Professor Antonio Bertoletti, Institute for Clinical Sciences at Agency for Science, Technology and Research (A*STAR)) were cultured in RPMI1640 medium (RPMI, HyClone, Utah, USA) supplemented with 10% fetal bovine serum (FBS), 1% (w/v) sodium pyruvate, 1% (w/v) N-2-hydroxy-ethylpiperazine-N'-2-ethanesulfonic acid (HEPES), 1% (w/v) penicillin/streptomycin at 37 $^{\circ}$C in humidified atmosphere of 5% (v/v) CO_2 incubator.

2.5.1 Cell preservation

HepG2 cells were resuspended in 1 mL freezing media (10% (v/v) DMSO in RPMI complete medium) and transferred to cryovial. Cells were stored at -80 $^{\circ}$C.

2.5.2 Cell preparation

HepG2 cells were collected using 0.25% trypsin/EDTA solution from container (T25 flask) and centrifuged at 1000 rpm for 5 mins. Cell pellets were resuspended in RPMI complete medium and stained by 0.4% tryphan blue stain. Cells were counted by hemacytometer. The number of viable cell was calculated as explained in previous section.

2.6 Intracellular trafficking of oxidized carbon nanoparticles in HEK293T cells

To intra-cellularly tracking the oxidized carbon nanoparticles in HEK293T cells, the cells were seeded in 8-well glass slide chamber (Lab-Tek II Chambered Coverglass, NUNC, NY, USA) at a density of 75000 cells per well (500 µL/ well) for 24 h and subjected to organelle staining (see below) and OCSs, OCTs and GOShs, treatment as follow:

2.6.1 Co-localization between oxidized carbon nanoparticles and endosome in HEK293T

Firstly, HEK293T cells were seeded in 8-well glass slide chamber at cell density of 75000 cells per well (500 µL/ well). After incubation for 2 and 4 h, the cells were incubated with 15 µL of endosome fluorescent dye reagent ($\lambda_{ex}/\lambda_{em}$ = 488/510 nm, CellLight® early endosome-GFP, Bacmam 2.0, Life Technologies, California, USA) at 37 °C under 5% (v/v) CO_2 for 18 h. Then, the cells were treated with TAMRA-labelled OCSs, OCTs and GOShs (depicted as $OCSs_{TAMRA}$, $OCTs_{TAMRA}$ and $GOShs_{TAMRA}$, $\lambda_{ex}/\lambda_{em}$ = 559/580 nm), of which working concentration in the cell suspensions were controlled at 10 µg/mL and incubated for 2 and 4 h at 37 °C under 5% CO_2. Next, the media were removed and the cells were washed twice with phosphate buffer saline (PBS, warmed at 37 °C). Next, the cells were fixed by treating with 100 µL of 4%(w/v) paraformaldehyde for 15 min and washed 3 times with PBS. Cell imaging was observed with Confocal laser scanning fluorescent microscope (CLSFM, FV10i-LIV) equipped with universal Plan Super Apochromat 60X phase contrast water immersion objective (Lens). Excitation was processed at 473 and 559 nm (MellesGriot Laser, Carlsbad, CA, USA) and emission was detected at 520 nm for endosome fluorescent dye reagent and 580 nm for $OCSs_{TAMRA}$, $OCTs_{TAMRA}$ and $GOShs_{TAMRA}$. Data was processed with FLUOVIEW 3.0 software.

2.6.2 Co-localization between oxidized carbon nanoparticles and lysosome in HEK293T

HEK293T cells were seeded in 8-well glass slide chamber at cell density of 75000 cells per well (500 µL/ well). The cells were treated with Fluorescein-labelled OCSs, OCTs and GOShs ($OCSs_{Flu}$, $OCTs_{Flu}$ and $GOShs_{Flu}$, final concentration at 10 µg/mL, $\lambda_{ex}/\lambda_{em}$ = 495/519 nm) for 4 and 6 h and incubated at 37 °C under 5% CO_2. Before cell fixation, lysosome was stained by adding 100 µL of 1000 nM of Lysotracker® Deep Red (150 nM as a final concentration, $\lambda_{ex}/\lambda_{em}$ = 650/668 nm, Life Technologies, California, USA), and incubation for 2 h. After finish incubation, the media of cells were

removed and washed 3 times with PBS. Next, the cells were fixed with 100 µl of 4%(w/v) paraformaldehyde for 15 min and washed 3 time with PBS. Nucleus was stained by incubation with 100 µL of 4'-6-diamidino-2'-phenylindole (DAPI, $\lambda_{ex}/\lambda_{em}$ = 358/461 nm), for 10 min at room temperature. 10 µg/ml of DAPI was used as final concentration of staining media. Sample was washed 3 times with PBS to remove excess dye, FV10i-LIV was used to observe cell imaging.

2.6.3 Co-localization between oxidized carbon nanoparticles, endoplasmic reticulum (ER) and golgi apparatus (GI) in HEK293T

Before the experiment, HEK293T cells were seeded in 8-well glass slide chamber at cell density of 75000 cells per well (500 µL/ well) and plated for 6 h. After that, the cells were incubated with 15 µL of ER fluorescent dye reagent ($\lambda_{ex}/\lambda_{em}$ = 488/510 nm, CellLight® ER-GFP, Bacmam 2.0, Life Technologies, California, USA) at 37 °C under 5% (v/v) CO_2, for 18 h. Next, the cells were treated with $OCSs_{TAMRA}$, $OCTs_{TAMRA}$ and $GOShs_{TAMRA}$ and incubated for 4 and 6. 10 µg/ml of TAMRA-labelled oxidized carbon nanoparticles were used as final concentration in cell suspensions. Before cell fixation, 20 µL of, Alexa Fluor 647 conjugated lectin GS-II (25 µg of, Alexa Fluor 647 conjugated lectin GS-II was dissolved in 1 mL of 1 mM $CaCl_2$ aqueous buffer, $\lambda_{ex}/\lambda_{em}$ = 650/668 nm, Life Technologies, California, USA), was added for GI staining, and incubated for 2 h. After finish incubation, the media were removed and washed 3 times with warm PBS. Finally, the cells were fixed with 100 µl of 4%(w/v) paraformaldehyde for 15 min and washed 3 times with PBS. Samples were imaged by using FV10i-LIV.

2.7 Intracellular trafficking of oxidized carbon nanoparticles in RAW264.7 cells

To intra-cellularly tracking the oxidized carbon nanoparticles in RAW264.7 cells, the cells were seeded in 8-well glass slide chamber at a density of 50000 cells per well (500 µL/ well) for 24 h and subjected to organelle staining (see below) and OCSs, OCTs and GOShs, treatment as follow:

2.7.1 Co-localization between oxidized carbon nanoparticles and endosome in RAW264.7

RAW264.7 cells were seeded in 8-well glass slide chamber at a density of 50000 cells per well (500 µL/ well). The cells were incubated with Fluorescein-labelled oxidized carbon nanoparticles (OCSs$_{Flu}$, OCTs$_{Flu}$ and GOShs $_{Flu}$), for 15 min, 30 min, 1 h and 2 h, at 37 °C under 5% (v/v) CO_2. 30 µg/ml of OCSs$_{Flu}$, OCTs$_{Flu}$ and GOShs $_{Flu}$ was used as final concentration in cell suspensions. After incubation, the media were removed. The cells were washed 3 times with PBS. Next, RAW26.47 cells were fixed with 100 µl of 4%paraformaldehyde for 15 min. After cell fixation, the cells were permeated with 100 µL of 0.2%(v/v) Triton-X 100 and incubated for 3 min. Blocking Fc receptor solution was prepared by mixing 10 µl of 2.4G2 suspension and 900 µL of 10% (v/v) fetal bovine serum (FBS). The cells were incubated with 100 µL of blocking solution for 20 min and washed 3 times with PBS. Next, the cells were incubated with 100 µL primary antibody for 1 h and washed 3 times with PBS. Primary antibody was prepared by mixing 1 µL of EEA1 antibody (EEA1 (C45B10) Rabbit mAb, IF-IC 1:100, Cell Signaling Technology, USA) with 100 ul of 1.5% (v/v) FBS. Then, secondary antibody was prepared by mixing 1 µL of Alexa Fluor 555 Conjugated with anti-Rabbit IgG (H+L), F(ab')$_2$ Fragment ($\lambda_{ex}/\lambda_{em}$ = 559/580 nm, IF-IC 1:1000, Cell Signaling Technology, USA) with 1.5% (v/v) FBS. 100 µL of secondary antibody was added to samples and incubated in the dark for 1 h. After incubaion with secondary antibody, samples were washed 3 times with PBS. Nucleus was stained by incubation 100 µL of DAPI for 10 min at room temperature and washed 3 times with PBS. 10 µg/ml of DAPI was used as final concentration for staining media. Elimination of excess DAPI were removed by washing with PBS 3 times. Finally, samples were visualized under ZEISS LSM800 confocal laser scanning fluorescent microscope (ZEISS LSM800) (Carl Zeiss Microscopy, NY., USA.) and data were processed with ZEN lite software.

2.7.2 Co-localization between oxidized carbon nanoparticles and lysosome in RAW264.7

Firstly, RAW264.7 cells were seeded in 8-well glass slide chamber at a density of 50000 cells per well (500 µL/ well). The cells were incubated with OCSs$_{Flu}$, OCTs$_{Flu}$ and GOShs s$_{Flu}$ for 2, 4 and 6 h at 37 ℃ under 5% (v/v) CO$_2$. Before cell fixation, lysosomes were stained by adding 100 µL of 1000 nM of Lysotracker$^{Ⓡ}$ Deep Red into cell suspensions and incubated for 2 h. After that, media were removed and the cells were washed with PBS 2 times. Then, the cells were fixed with 100 µL of 4%(w/v) paraformaldehyde for 15 min and washed with PBS 3 times. Nucleus were stained 100 µL of DAPI for 10 min at room temperature. 10µg/ml of DAPI was used final concentration in staining media. Excess dyes were removed by washing with PBS 3 times. Finally, the cells were imaged by using FVi10-LIV.

2.7.3 Co-localization between oxidized carbon nanoparticles and autophagosomes in RAW264.7

RAW264.7 cells were seeded in 8-well glass slide chamber at a density of 50000 cells per well (500 µL/ well). The cells were incubated with OCSs$_{Flu}$ for 4 h at 37 ℃ under 5% (v/v) CO$_2$. 30 µg/ml of OCSs$_{Flu}$ was used as final concentration in cell suspension. After incubation, media were removed and the cells were washed 3 times with PBS. Next, the cells were fixed with 100 µL of 4% (w/v) paraformaldehyde for 15 min and washed 3 times with PBS. The cells were permeated with 100 µL of 0.2% (v/v) Triton-X 100 for 3 min. The cells were blocked Fc receptor by incubation with blocking solution (as shown in section 2.7.1) for 20 min. Primary antibody was prepared by mixing 1 µL of LC3b antibody (IF-IC 1:100, Cell Signaling Technology, USA) and 900 µL of 1.5 (v/v) FBS. The cells were incubated with 100 µL of primary antibody for 1 h and washed 3 times with PBS. Then, the cells were incubated with 100 µL of secondary antibody (preparation was shown in section 2.7.1) for 1 h and washed 3 times with PBS. Nucleus was stained by incubation with 100 µL of DAPI at room temperature. 10 µg/ml of DAPI was used as final concentration in staining media. Excess DAPI were removed by washing with PBS 3 times. Finally, samples were visualized under ZEISS

LSM800 confocal laser scanning fluorescent microscope (ZEISS LSM800) (Carl Zeiss Microscopy, NY., USA.) and data were processed with ZEN lite software.

2.7.4 Co-localization between oxidized carbon nanoparticles and endoplasmic reticulum (ER) in RAW264.7

RAW264.7 cells were seeded in 8-well glass slide chamber at a density of 50000 cells per well (500 µL/ well). The cells were incubated with $OCSs_{TAMRA}$, $OCTs_{TAMRA}$ and GOShs $_{TAMRA}$ for 4 h at 37 °C under 5% (v/v) CO_2. 30 µg/ml of $OCSs_{TAMRA}$, $OCTs_{TAMRA}$ and GOShs $_{TAMRA}$ were used as final concentration in cell suspension. Before finishing incubation, the cells were stained ER by ER-tracker^{TM} Green glibenclamide BODIPY®FL (1 mM of stock solution in DMSO, $\lambda_{ex}/\lambda_{em}$ = 504/511 nm, Invitrogen, UK), of which working concentration in cell suspension was controlled at 10 µM for 4 h. The media were removed and washed 2 times with complete media. After that, the cells were visualized with ZEISS LSM800, immediately.

2.7.5 Co-localization between oxidized carbon nanoparticles and golgi apparatus (GI) in RAW264.7

RAW264.7 cells were seeded in 8-well glass slide chamber at cell density of 50000 cells per well (500 µL/ well). The cells were incubated with $OCSs_{Flu}$, $OCTs_{Flu}$ and GOShs $_{Flu}$ for 4 and 6 h at 37 °C under 5% (v/v) CO_2. 30 µg/ml of $OCSs_{Flu}$, $OCTs_{Flu}$ and GOShs $_{Flu}$ was used as final concentration in cell suspension. Before cell fixation, the cells were treated with 20 µL of Alexa Fluor 647 conjugated lectin GS-II and incubated for 2 h. After finish incubation, media were removed and the cells were washed 3 times with PBS. Then, the cells were fixed with 100 µL of 4%(w/v) paraformaldehyde for 15 min. Nucleus were stained 100 µL of DAPI for 10 min at room temperature. 10µg/ml of DAPI was used final concentration in staining media. Next, the cells were washed 3 times with PBS. Finally, the cells were visualized under FV10i-LIV.

2.8 Intracellular trafficking of oxidized carbon nanoparticles in HepG2 cells

To intra-cellularly tracking the oxidized carbon nanoparticles in HepG2 cells, the cells were seeded in 8-well glass slide chamber at a density of 50000 cells per well (500 μL/ well) for 24 h and subjected to organelle staining (see below) and OCSs, OCTs and GOShs, treatment as follow:

2.8.1 Co-localization between oxidized carbon nanoparticles and endosome in HepG2

Firstly, HepG2 cells were seeded in 8-well glass slide chamber at cell density of 50000 cells per well (500 μL/ well) and incubated at 37 °C under 5% (v/v) CO_2. The cells were treated with $OCSs_{Flu}$, $OCTs_{Flu}$ and $GOShs_{Flu}$ for 2 h at 37 °C under 5% (v/v) CO_2. After incubation, the media were removed and the cells were washed 3 times with PBS. Next, HepG2 cells were fixed with 4%paraformaldehyde and permeated by using 0.2% (v/v) Triton-X 100, as shown in section 2.7.1. Blocking solution were prepared by mixing 100 μL of FBS and 900 μL of PBS. The cells were incubated with 100 μL of blocking solution for 20 min and washed 3 times with PBS. After that, the cells were incubated with the EEA1 antibody for 1 h and washed 3 times with PBS. Then, 100 μL of secondary antibody was added into cells container and incubated for 1 h in the dark. Preparation of EEA1 antibody and secondary antibody were described in section 2.7.1. Next, the cells were washed 3 times with PBS. Nucleus was stained by using 100 μL of DAPI which working concentration in the staining media was controlled at 10 μg/mL and incubated for 10 min at room temperature. Excess DAPI were eliminated by washing with PBS 3 times. Finally, samples were visualized under ZEISS LSM800.

2.8.2 Co-localization between oxidized carbon nanoparticles and lysosome in HepG2

HepG2 cells were seeded in 8-well glass slide chamber at cell density of 50000 cells per well (500 µL/ well). The cells were incubated with $OCSs_{Flu}$, $OCTs_{Flu}$ and $GOShs_{Flu}$ for 4 and 6 h and incubated at 37 °C under 5% (v/v) CO_2. Before cell fixation, lysosome was stained by using 100 µL of 1000 nM of Lysotracker® Deep Red, add into cell suspensions and incubated for 2 h. After finish incubation, media were removed and the cells were washed with PBS 3 times. Next, the cells were fixed with 100 µL of 4% paraformaldehyde for 15 min and washed with PBS 3 times. Nucleus were stained with 100 µL of DAPI, which working concentration was controlled at 10 µg/ml in staining media and incubated for 10 min at room temperature. Excess dyes were removed by washing with PBS 3 times. Finally, the cells were visualized under ZEISS LSM800.

2.8.3 Co-localization between oxidized carbon nanoparticles, endoplasmic reticulum (ER) and golgi apparatus (GI) in HepG2

HepG2 cells were seeded in 8-well glass slide chamber at cell density of 50000 cells per well (500 µL/ well). The cells were stained ER by ER-tracker™ Green glibenclamide BODIPY®FL (1 mM of stock solution in DMSO, $\lambda_{ex}/\lambda_{em}$ = 504/511 nm, Invitrogen, UK), which working concentration of ER tracker was controlled at 10 µM in cell suspension and incubated for 4 h at 37 °C under 5% (v/v) CO_2. The cells were treated with $OCSs_{TAMRA}$, $OCTs_{TAMRA}$ and $GOShs_{TAMRA}$ and incubated for 4 h at 37 °C under 5% (v/v) CO_2. 30 µg/ml of TAMRA-labelled oxidized carbon nanoparticles were used as final concentration in cell suspension. Before finishing incubation, 20 µL of Alexa Fluor 647 conjugated with lectin GS-II was added into cell suspension and continuously incubated for 2h. After finishing incubation, media were removed and the cells were washed 3 times with PBS. Finally, the cells were visualized under FV10i-LIV, immediately.

CHAPTER III

RESULTS AND DISCUSSION

3.1 Synthesis and characterization of oxidized carbon nanospheres (OCSs), oxidized carbon nanotubes (OCTs) and oxidized graphene sheets (GOShs)
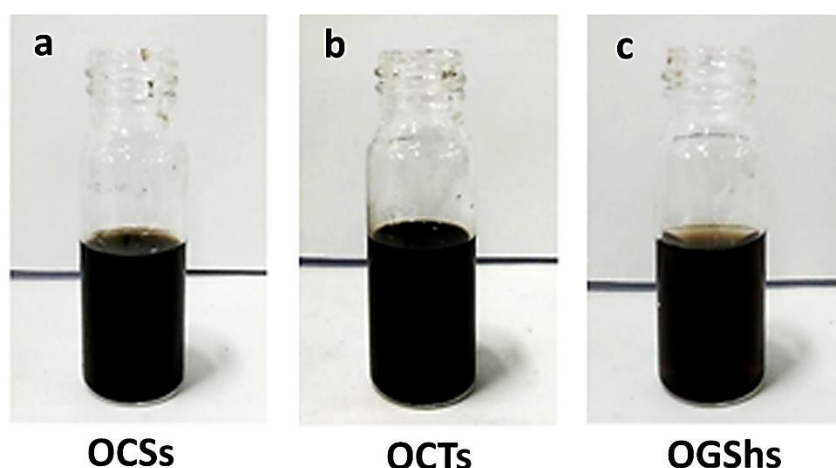
Figure 3.1: Suspension of oxidized carbon nanoparticles, (a) OCSs, (b) OCTs and (c) GOShs.

Oxidized carbon nanospheres (OCSs) and graphene oxide sheets (GOShs) were prepared from oxidation of graphite. Graphite powder were mixed with sodium nitrate and dispersed in concentrated sulfuric acid. Sonication was carried on the mixture became homogenous. Then, the mixture was added with KMnO$_4$, as oxidizing agent. After that, the mixture was added with deionized water. Heat was generated during this time. The mixture which was opaque suspension, was transformed into brown opaque suspension, air bubbles were also observed. Then, the reaction was added with 5% (v/v) H$_2$O$_2$ for elimination of KMnO$_4$. Finally, the mixture was subjected to multi-step centrifugation, as shown in **Table 3.1**. GOShs was precipitated by centrifugation at 21100 g for 15 min. Dispersing GOShs in water gave a brown colloidal suspension (**Figure 3.1c**). OCSs was collected from the supernatant as a dark brown colloidal suspension (**Figure 3.1a**). OCTs could be isolated to be free of GOShs. Hence, OCTs was synthesized from single-walled carbon nanotubes (SWCNTs). The reaction

was carried out as the reaction used in preparation of OCSs and GOShs, but without sonication. SWCNTs was mixed with sodium nitrate and dispersed in sulfuric acid. Then, the mixture was added with deionized water. After that, the mixture was added with 5% (v/v) H_2O_2. Finally, the mixture was centrifuged at 11300 g for 15 min and supernatant was collected as OCTs. OCTs was dark colloidal suspension (**Figure 3.1b**).

Table 3.1: Gradient centrifugation

Rotation speed (RCF)	Time (min)	Precipitate
9400 g	10	Big sized carbon debris
11300 g	15	Big tubes and sheets
21000 g	15	GOShs
37000 g	30	OCSs (supernatant)

Morphology of OCSs, OCTs and GOShs were verified by scanning electron microscopy (SEM) and transmission electron microscopy (TEM) as shown in **Figure 3.2**. OCSs showed spherical shape with diameter 100-200 nm, whereas OCTs showed tubular shape with aspect ratio of 10 and an average length of 1 μm, and GOShs showed sheet-shaped with size of 0.5 × 0.5 μm. Moreover, average hydrodynamic diameter and zeta potential of OCSs, OCTs and GOShs were obtained by dynamic light scattering analysis (DLS). The data were shown in **Table 3.2**.

Table 3.2: Average hydrodynamic diameter of OCSs, OCTs and GOShs

	GOShs	OCTs	OCSs
Hydrodynamic diameters (nm) ±SD	266.9 ±5	243.6 ±17	154.6 ±30
PDI	0.25	0.78	0.33
Zeta potential (mV)	-40	-35.5	-32.6

.

OCSs, OCTs and GOShs were characterized for their functional groups by infared spectroscopy OCSs, OCTs and GOShs showed similar pattern of infared spectra with O-H streching (3130-3300 cm^{-1}), C=O stretching (1710-1730 cm^{-1}), and C=C streching (1605-1625 cm^{-1}), as shown in **Figure 3.3**. In addition, raman spectroscopy shows graphitic carbon band (G-band) and disordered carbon band at 1590 cm^{-1} for G-band and 1360 cm^{-1} for D-band (**Figure 3.4**). D-band and G-band represent sp^2-carbon and sp^3 carbon, respectively. The results revealed that OCSs, OCTs and GOShs contain the sp^2-carbon network in their structure as similar to their starting materials. However, oxidation produced sp^3 carbon on their structures. All three shapes of the oxidized carbon nanoparticles (OCNs) show carboxylic acid (-COOH) and hydroxyl groups (-OH).
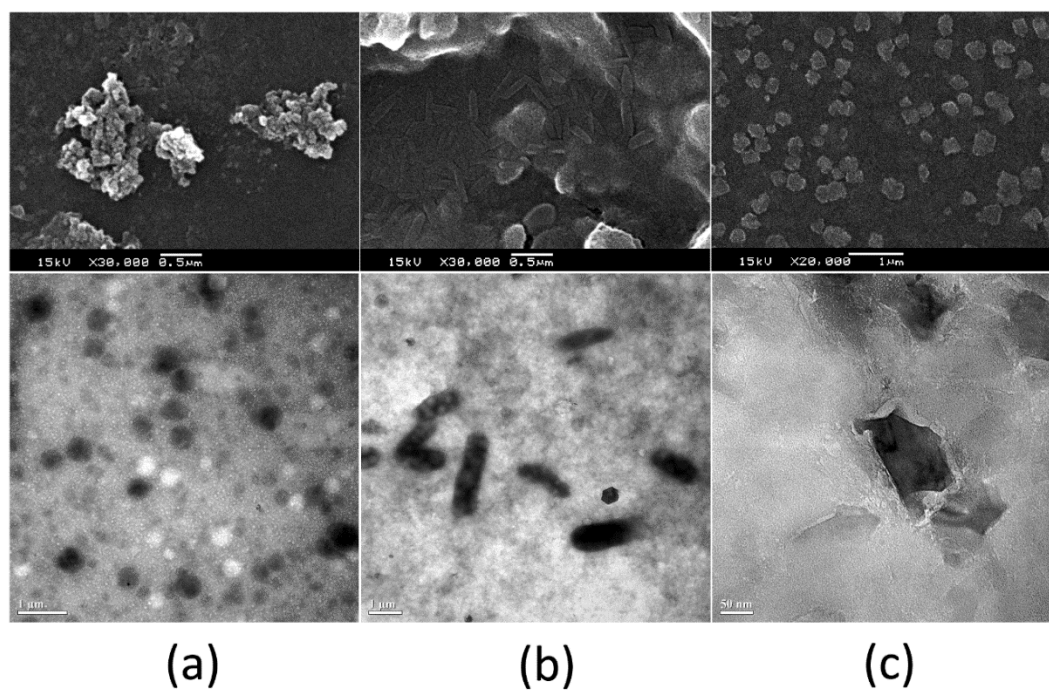
Figure 3.2: SEM (top) and TEM (bottom) images of (a) OCSs, (b) OCTs and (c) GOShs.

Table 3.3: Peak height ratio of D/G band

	Peak height ratio of D/G
Graphite powder	0.30
Single-walled carbon nanotubes (SWCNTs)	0.60
GOShs	0.93
OCTs	0.86
OCSs	0.92
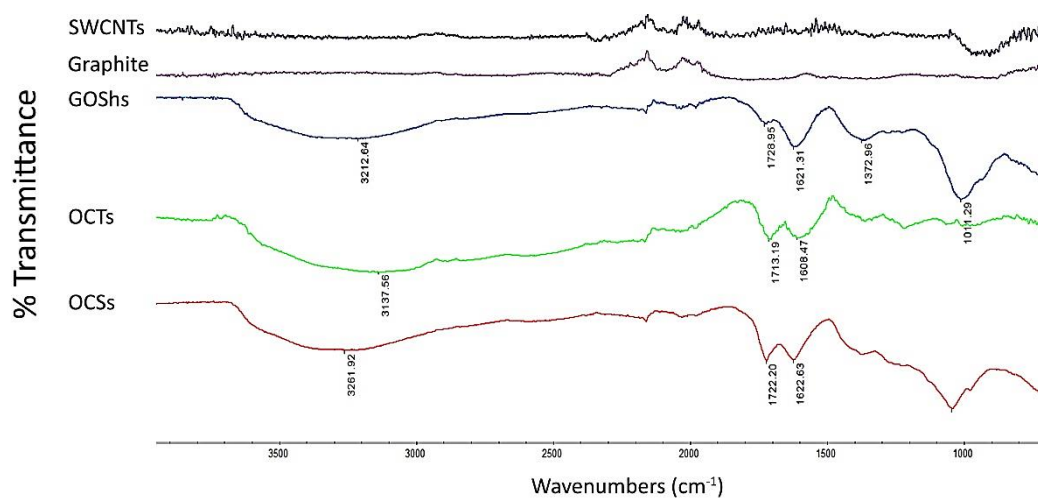
Figure 3.3: Infrared spectra of graphite powder, SWCNTs, GOShs, OCTs and OCSs
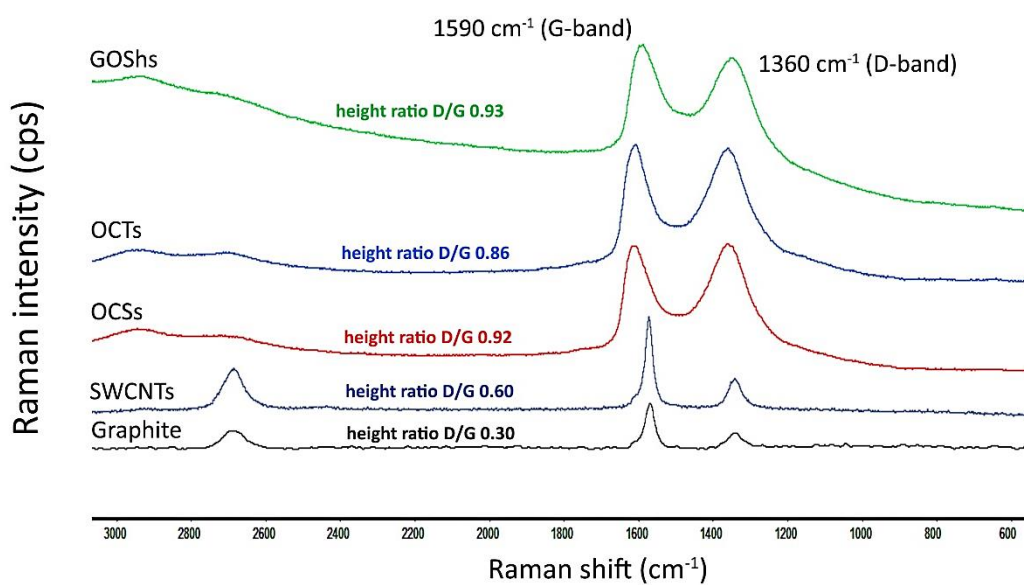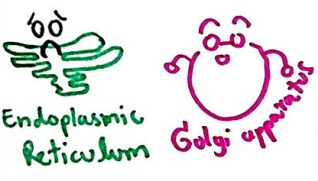
Figure 3.4: Raman spectra of graphite powder, SWCNTs, GOShs, OCTs and OCSs

3.2 Investigation of intracellular trafficking

In this research, intracellular trafficking of the three shapes of oxidized carbon nanoparticles (OCNs) were investigated in three different cells; human embryonic kidney cells (HEK293T) as a representative of normal cells [50-52]. Mouse macrophage celss (RAW264.7) as a representative of immune cells and antigens presenting cells [53, 54]. Human liver cancer cells (HepG2) as representative of cancer cells. Two major pathways vital for cell function; endocytic pathway as route for internalization of essential things and exocytic pathway as route for shuttling things out of the cells, were have investigated (**Table 3.3**).

Table 3.4: Cellular compartment in endocytic and exocytic pathway.

3.2.1 Intracellular trafficking of oxidized carbon nanoparticles in HEK293T cells

3.2.1.1 Co-localization between oxidized carbon nanoparticles and endosome in KEK293T

To visualized co-localization between oxidized carbon nanoparticles and endosome, HEK293T cells were incubated with CellLight® early endosome-GFP, the dye that specific to endosome, and treated with 10 μg/ml of OCSs$_{TAMRA}$, OCTs$_{TAMRA}$ and GOShs $_{TAMRA}$ at 37 °C under 5% CO_2 for 2 and 4 h, then the cells were fixed and monitored by CLSFM. **Figure 3.5** showed fluorescent signals of various dye. Column a-d show nucleus, endosome, TAMRA-labelled OCNs and merge fluorescent signals. Row 1-4 display untreated cells, the cells that were treated with GOShs, OCTs and OCSs, respectively. Signals of all the three shaped OCNs did not co-localized with endosome signals. Hence, all three shapes of OCNs were probably internalized into the cells without going through the endosome.

Figure 3.5: Intracellular trafficking of TAMRA-labelled oxidized carbon nanoparticles and endosome in HEK293T cells: Cells incubated with no particels (row 1), GOShs $_{TAMRA}$ (row 2), OCTs$_{TAMRA}$ (row 3) and OCSs$_{TAMRA}$ (row 4). Image in the fluorescence mode showing nucleus staining with DAPI (blue, $\lambda_{ex}/\lambda_{em}$ = 405/450 nm, column a), CellLight® early endosome-GFP (green, $\lambda_{ex}/\lambda_{em}$ = 488/510 nm, column b), TAMRA-labelled oxidized carbon nanoparticles (red, $\lambda_{ex}/\lambda_{em}$ = 559/580 nm, column c), and merged fluorescent signals (column d).

3.2.1.2 Co-localization between oxidized carbon nanoparticles and lysosome in HEK293T

HEK293T cells were treated with 10 µg/ml of oxidized carbon nanoparticles at 37 °C under 5% CO_2 for 4 and 6 h. The cells were stained with lysotracker and DAPI, respectively. **Figure 3.6** display fluorescent signals from nucleus staining (column a), fluorescein-labelled OCNs (column b), lysosome staining (column c) and merged fluorescent signal (column d). Row 1-4 exhibited untreated cells, the cells treated with GOShs, OCTs and OCSs, respectively. Some signals of all three shaped OCNs co-localized with lysosome signals. Therefore, we concluded that all three shapes of OCNs were trafficked through lysosomal compartment.

Figure 3.6: Intracellular trafficking of fluorescein-labelled oxidized carbon nanoparticles and lysosome in HEK293T cells: Cells incubated with no particels (row 1), GOShs $_{Flu}$ (row 2), OCTs$_{Flu}$ (row 3) and OCSs$_{Flu}$ (row 4). Image in the fluorescence mode showing nucleus staining with DAPI (blue, $\lambda_{ex}/\lambda_{em}$ = 405/450 nm, column a), Fluorescein-labelled oxidized carbon nanoparticles (green, $\lambda_{ex}/\lambda_{em}$ = 497/519 nm, column b), lysotracker (red, $\lambda_{ex}/\lambda_{em}$ = 650/668 nm, column c), and merged fluorescent signals (column d). White arrowhead indicated localization of OCNs and lysosome.

3.2.1.3 Co-localization between oxidized carbon nanoparticles, endoplasmic reticulum (ER) and golgi apparatus

HEK293T cells were incubated with CellLight® ER-GFP, dye that specific to endoplasmic reticulum (ER), and Alexa Fluor 647 conjugated lectin GS-II, dye that specific to golgi apparatus, then the cells were treated with 10 μg/ml of OCNs at 37 °C under 5% CO_2 for 4 and 6h. In **Figure 3.7** represent ER staining (column a), TAMRA-labelled oxidized carbon nanoparticles (column b), golgi apparatus staining (column c) and merged fluorescent signals (column d). Row 1-4 exhibited untreated cells, the cells treated with GOShs, OCTs and OCSs, respectively. Signal of all three shaped OCNs co-localized with signal of golgi apparatus and did not co-localized with ER. Hence, three shapes of OCNs were trafficked through golgi apparatus and were not in ER.
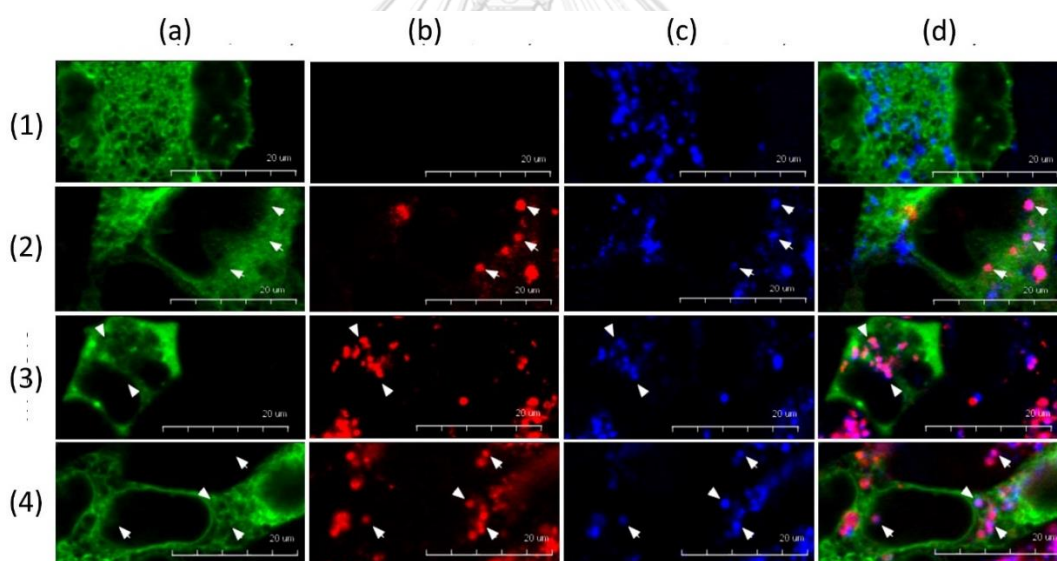
Figure 3.7: Intracellular trafficking of TAMRA-labelled oxidized carbon nanoparticles endoplasmic reticulum and golgi apparatus in HEK293T cells: Cells incubated with no particels (row 1), GOShs$_{TAMRA}$ (row 2), OCTs$_{TAMRA}$ (row 3) and OCSs$_{TAMRA}$ (row 4). Image in the fluorescence mode showing ER staning by CellLight® ER-GFP (green, $\lambda_{ex}/\lambda_{em}$ = 488/510 nm, column a), TAMRA-labelled oxidized carbon nanoparticles (red, $\lambda_{ex}/\lambda_{em}$ = 559/580 nm, column b), golgi apparatus staining by Alexa Fluor 647 conjugated lectin GS-II (blue, $\lambda_{ex}/\lambda_{em}$ = 650/668 nm, column c), and merged fluorescent signals (column d). White arrowhead indicated localization of OCNs and golgi apparatus.

3.2.2 Intracellular trafficking of oxidized carbon nanoparticles in RAW264.7 cells

3.2.2.1 Co-localization between oxidized carbon nanoparticles and endosome in RAW264.7
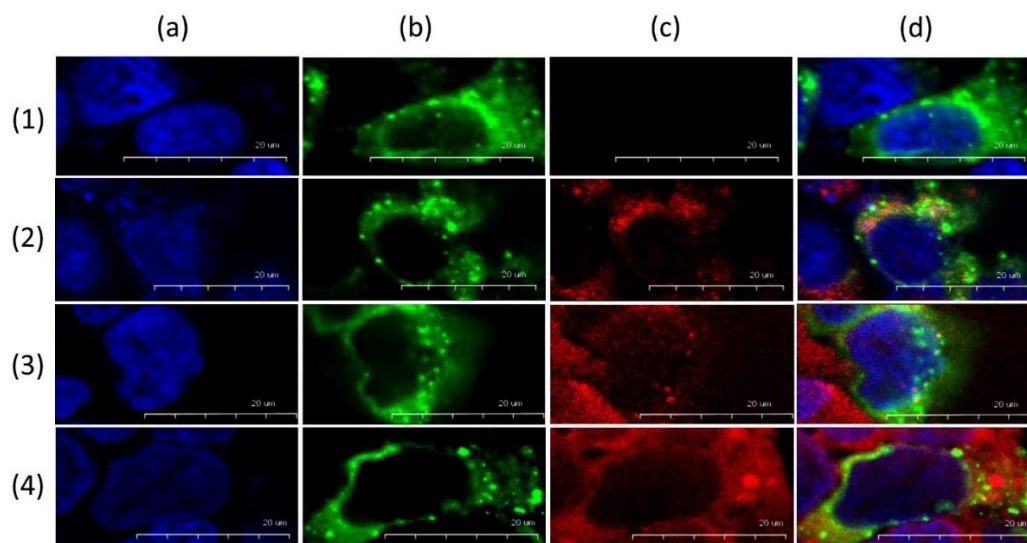

Figure 3.8: Intracellular trafficking of fluorescein-labelled oxidized carbon nanoparticles and endosome in RAW264.7 cells: Cells incubated with no particels (row 1), GOShs$_{Flu}$ (row 2), OCTs$_{Flu}$ (row 3) and OCSs$_{Flu}$ (row 4). Image in the fluorescence mode showing nucleus staining with DAPI (blue, $\lambda_{ex}/\lambda_{em}$ = 405/450 nm, column a), fluorescein-labelled oxidized carbon nanoparticles (green, $\lambda_{ex}/\lambda_{em}$ = 488/510 nm, column b), endosome staining with EEA1 antibody (red, $\lambda_{ex}/\lambda_{em}$ = 555/561 nm, column c), and merged fluorescent signals (column d).

RAW264.7 cells were incubated with 30 μg/ml of oxidized carbon nanoparticles at 37 °C under 5% CO_2 for 2 h, the cells were fixed and treated with EEA1 antibody (IF-IC 1:100) for endosome staining, respectively. **Figure 3.8** showed fluorescent signals of various dye. Column a-d show nucleus, fluorescein-labelled OCNs, endosome and merge fluorescent signals. Row 1-4 display untreated cells, the cells that were treated with GOShs, OCTs and OCSs, respectively. The results in **Figure 3.8** revealed signals of all three shaped OCNs did not co-localized with endosome signals. Therefore, OCSs, OCTs and GOShs were probably internalized into the cells without going through endosome.

3.2.2.2 Co-localization between oxidized carbon
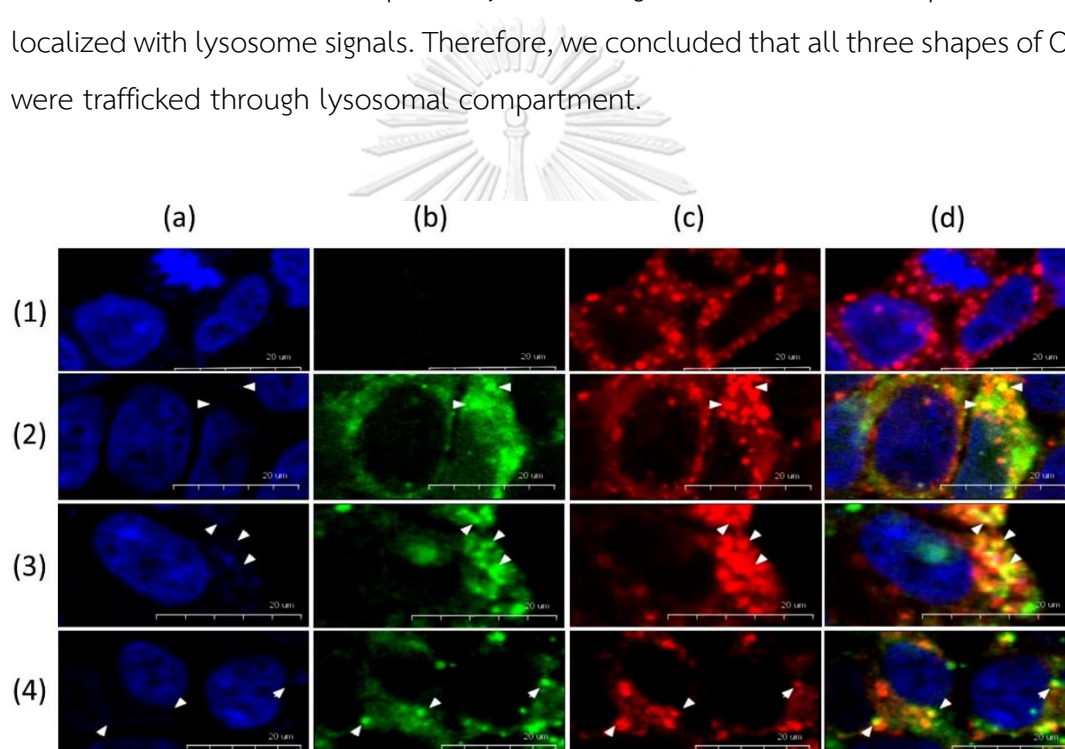nanoparticles and lysosome in RAW264.7
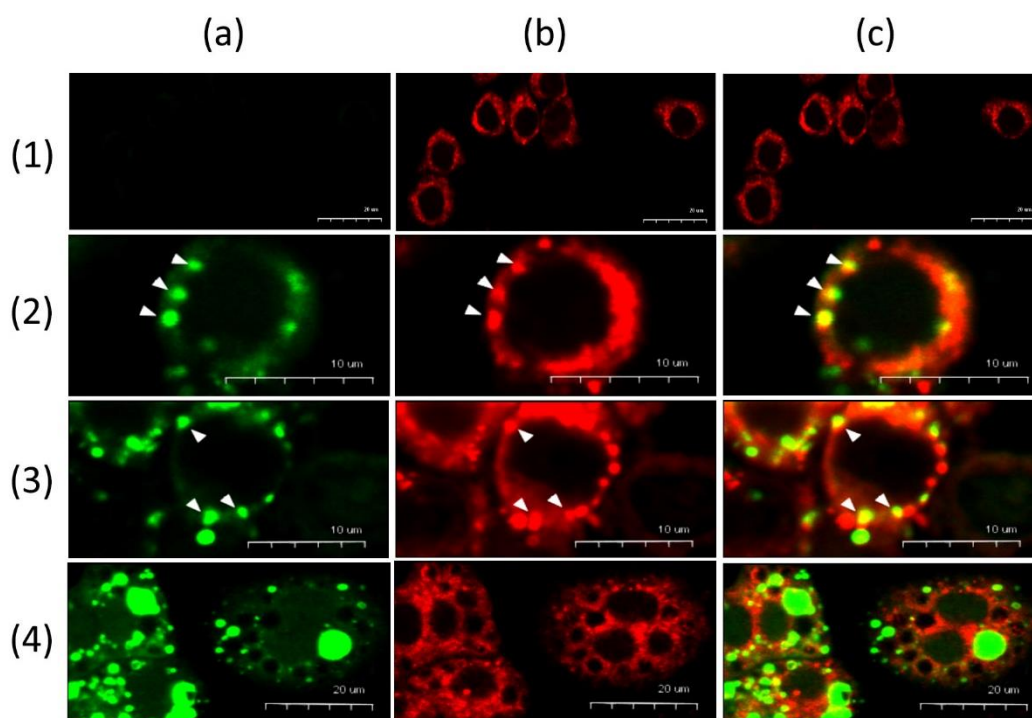
Figure 3.9: Intracellular trafficking of fluorescein-labelled oxidized carbon nanoparticles and lysosome in RAW264.7 cells: Cells incubated with no particels (row 1), GOShs$_{Flu}$ (row 2), OCTs$_{Flu}$ (row 3) and OCSs$_{Flu}$ (row 4). Image in the fluorescence mode showing fluorescein-labelled oxidized carbon nanoparticles (green, $\lambda_{ex}/\lambda_{em}$ = 497/519 nm, column a), lysotracker (red, $\lambda_{ex}/\lambda_{em}$ = 650/668 nm, column b), and merged fluorescent signals (column c). White arrowhead indicated co-localization in lysosome. White arrowheads indicated localization of OCNs and lysosomes.

RAW264.7 cells were treated with $OCSs_{Flu}$, $OCTs_{Flu}$ and $GOShs_{Flu}$ at 37 °C under 5% CO_2 which their working concentration was controlled at 30 µg/ml for 6 h, then the cells were incubated with lysotracker and fixed. Finally, the cells were observed by CLSFM. **Figure 3.9** display signals of fluorescein-labelled three shaped OCNs (column a), lysotracker (column b) and merged fluorescent signals (column c). Row 1-4 display untreated cells, the cells that were treated with GOShs, OCTs and OCSs, respectively. GOShs and OCTs signals were localized in lysosome signals and signals of OCSs were not localized in lysosome. Hence, GOShs and OCTs were trafficked through lysosome and OCSs was not in lysosome.
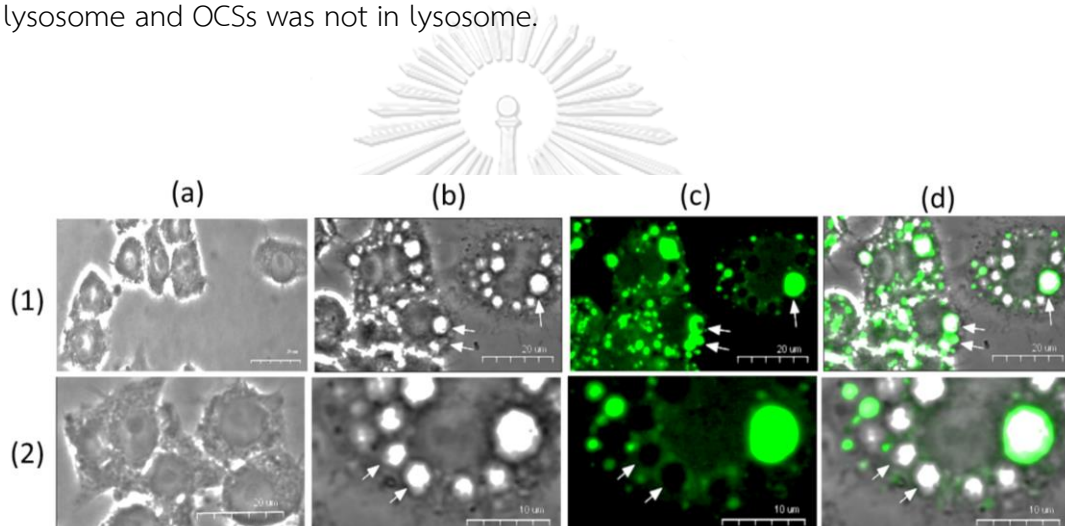
Figure 3.10: Cell images of untreated RAW264.7 cells (column a, row 1 and 2) and treated RAW264.7 cells with 30 µg/ml of OCSs for 6h (column b-d, row 1 and 2). Column b shows phase contrast. Column c shows fluorescent signal of $OCSs_{Flu}$ (green, $\lambda_{ex}/\lambda_{em}$ = 495/519 nm) and column d is merged images of b and c. White arrow in row 1 indicated vesicles that contained OCSs. White arrow in row 2 indicated vesicles that no fluorescent signals from $OCSs_{Flu}$.

3.2.2.3 Co-localization between oxidized carbon nanospheres and phagosome in RAW264.7

Generally, under stress condition, such as nutrient deprivation, pathogens infection [55], and diseases [56], autophagy can be induced in the cells. Vesicles were generated to entrap cytoplasm and organelles transformed into autophagosomes and then deliver to lysosome for degradation [34]. To investigate whether, the vesicle observed in **Figure 3.9 and 3.10** were autophagosomes, immunofluorescence assay was used. In the experiment, RAW264.7 cells were treated with fluorescein-labelled oxidized carbon nanospheres. After that, the cells were fixed and incubated with LC3b antibody (autophagosome marker [57]) and alexa fluor 561 conjugated secondary antibody. In addition, the cells were stained with DAPI. Finally, the cells were observed under CLSFM.
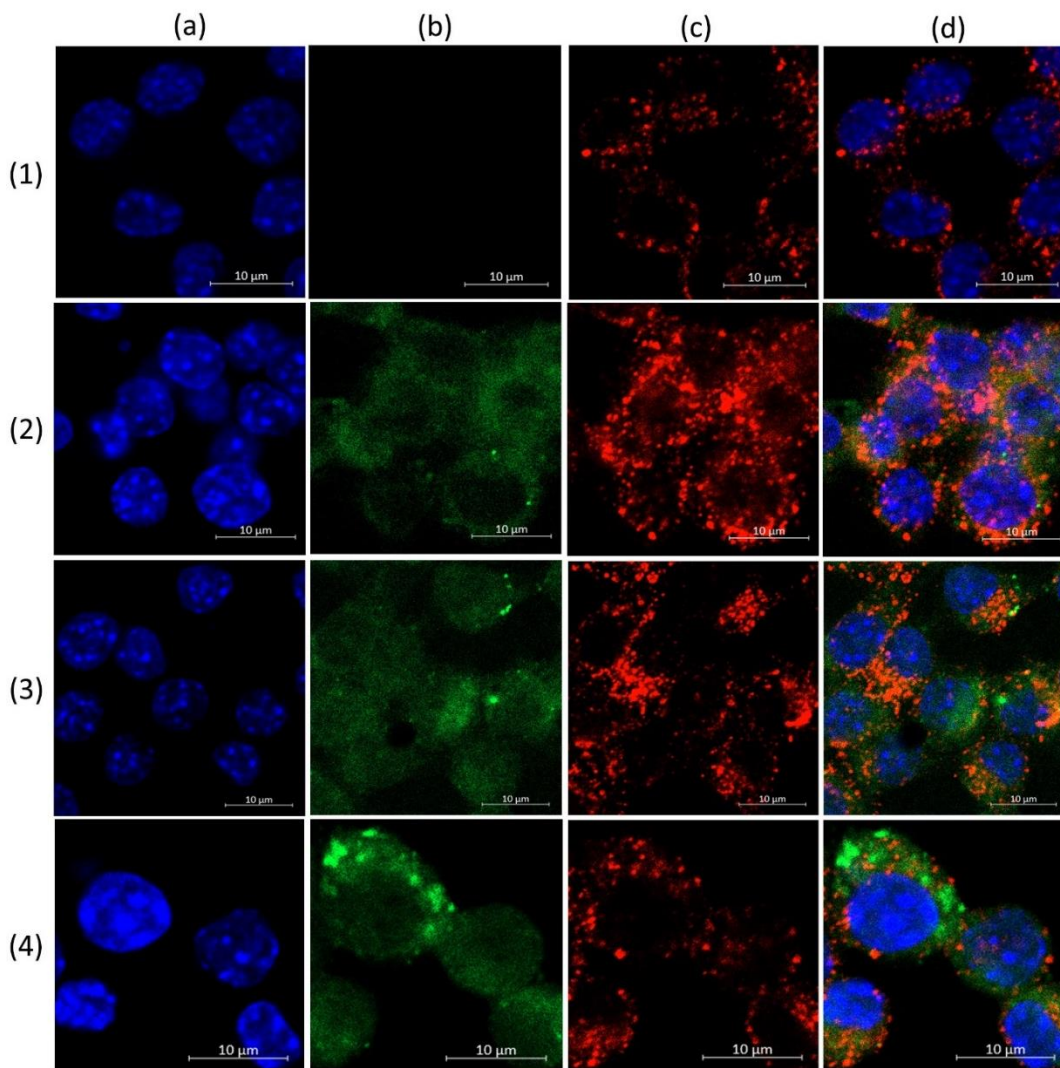
Figure 3.11: Intracellular trafficking of fluorescein-labelled oxidized carbon nanoparticles and autophagsome in RAW264.7 cells: Cells incubated with no particels (row 1) and OCSs$_{Flu}$ (row 2), Image in the fluorescence mode showing nucleus staining with DAPI (blue, $\lambda_{ex}/\lambda_{em}$ = 405/450 nm, column a), fluorescein-labelled oxidized carbon nanoparticles (green, $\lambda_{ex}/\lambda_{em}$ = 488/510 nm, column b), autophagosome staining with LC3b antibody (red, $\lambda_{ex}/\lambda_{em}$ = 555/561 nm, column c), and merged fluorescent signals (column d).

In **Figure 3.11** display various fluorescent signals from nucleus staining (column a) and OCSs$_{Flu}$ (column b) autophagosome staining (column c) and merged fluorescent signals (column d). OCSs signals appeared compartmental in cell cytoplasm, the OCSs signal did not localize with autophagosome signals (column d). This implies that OCSs were not entraped into autophagosome.

3.2.2.4 Co-localization between oxidized carbon nanoparticles and endoplasmic reticulum in RAW264.7
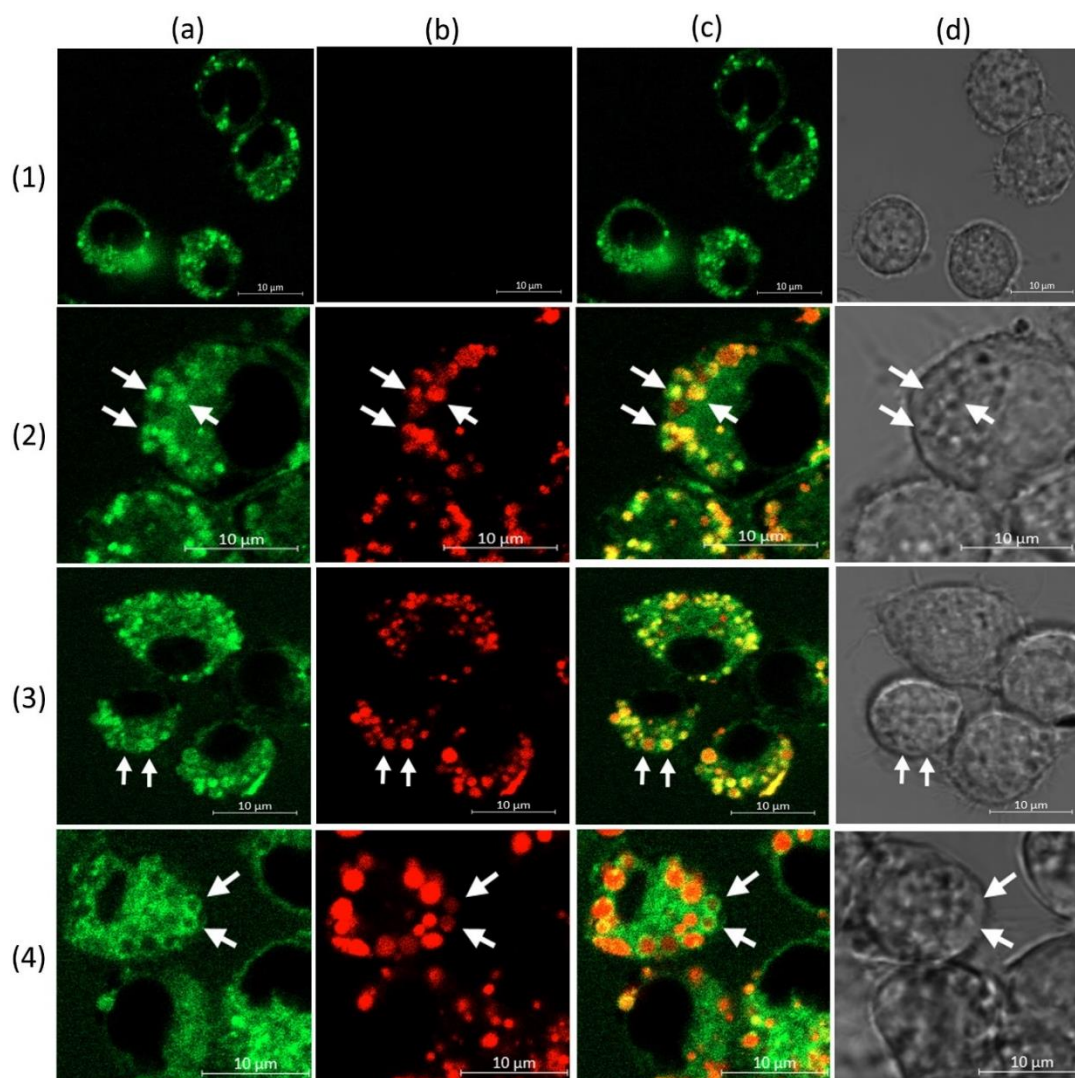
Figure 3.12: Intracellular trafficking of TAMRA-labelled oxidized carbon nanoparticles and endoplasmic reticulum (ER) in RAW264.7 cells: Cells incubated with no particels (row 1), GOShs$_{TAMRA}$ (row 2), OCTs$_{TAMRA}$ (row 3) and OCSs$_{TAMRA}$ (row 4). Image in the fluorescence mode showing ER staining with ER tracker (green, $\lambda_{ex}/\lambda_{em}$ = 504/511 nm, column a), TAMRA-labelled oxidized carbon nanoparticles (red, $\lambda_{ex}/\lambda_{em}$ = 559/580 nm, column b), merged fluorescent signals (column c), and DIC images of RAW264.7 (column d). White arrows indicated localization of OCNs and endoplasmic reticulum.

RAW264.7 cells were incubated with TAMRA-labelled OCNs CO_2, which their working concentration was controlled at 30 µg/ml, at 37 °C under 5% for 4 h. The cells were incubated with ER-tracker. After finish incubation, the cells were wash 2 times with complete media and immediately visualized during alive by CLSFM. **Figure 3.12** exhibited various fluorescent signal from ER staining (column a), TAMRA-labelled oxidized carbon nanoparticles (column b), merged fluorescent signals (column c) and DIC images of RAW264.7 cells (column d). Row 1-4 display untreated cells, the cells that were treated with GOShs, OCTs and OCSs, respectively. All signals of three shapes of oxidized carbon nanoparticles co-localized with ER signals. Thus, OCSs, OCTs and GOShs were trafficked through endoplasmic reticulum.

3.2.2.5 Co-localization between oxidized carbon nanoparticles and golgi apparatus in RAW264.7
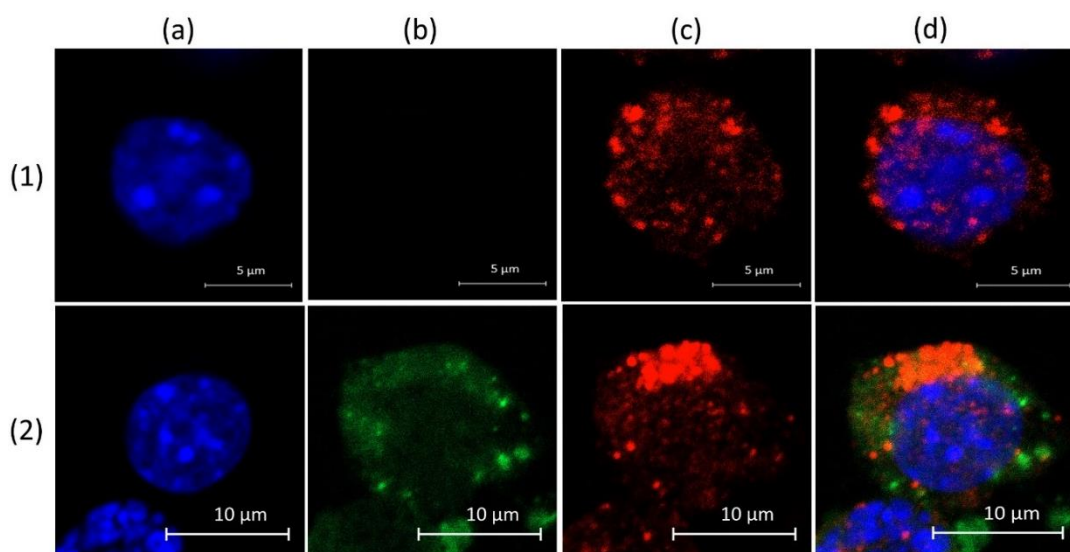

Figure 3.13: Intracellular trafficking of fluorescein-labelled oxidized carbon nanoparticles and golgi apparatus in RAW264.7 cells: Cells incubated with no particels (row 1), GOShs$_{Flu}$ (row 2), OCTs$_{Flu}$ (row 3) and OCSs$_{Flu}$ (row 4). Image in the fluorescence mode showing nucleus staining with DAPI (blue, $\lambda_{ex}/\lambda_{em}$ = 450/450 nm, column a), fluorescein-labelled oxidized carbon nanoparticles (green, $\lambda_{ex}/\lambda_{em}$ = 497/519 nm, column b), golgi apparatus staining by Alexa Fluor 647 conjugated lectin GS-II (red, $\lambda_{ex}/\lambda_{em}$ = 650/668 nm, column c) and merged fluorescent signals (column d), White arrows indicated localization of OCNs and golgi apparatus.

RAW264.7 cells were incubated 30 µg/ml of oxidized carbon nanoparticles, at 37 °C under 5% CO_2 for 4 and 6h. The cells were incubated with AF647-conjugated with lectin-GSII and fixed for observation under CLSFM. **Figure 3.13** display fluorescent signals from nucleus staining (column a), fluorescein-labelled oxidized carbon nanoparticles (column b), golgi apparatus staining (column c) and merged fluorescent signals (column d). Row 1-4 display untreated cells, the cells that were treated with

GOShs, OCTs and OCSs, respectively. some signals of all three shaped OCNs signals co-localized with golgi apparatus signals (column d). Therefore, three shapes of OCNs were trafficked through golgi apparatus.

3.2.3 Intracellular trafficking of oxidized carbon nanoparticles in HepG2 cells

3.2.3.1 Co-localization between oxidized carbon nanoparticles and endosome in HepG2
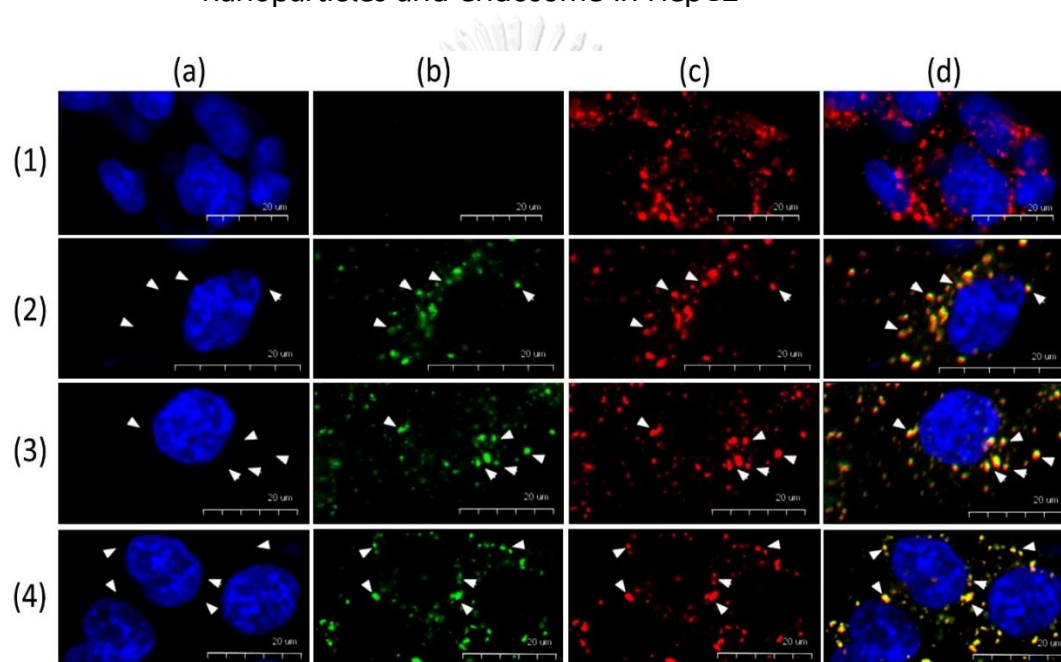
Figure 3.14: Intracellular trafficking of fluorescein-labelled oxidized carbon nanoparticles and endosome in HepG2 cells: Cells incubated with no particels (row 1), GOShs$_{Flu}$ (row 2), OCTs$_{Flu}$ (row 3) and OCSs$_{Flu}$ (row 4). Image in the fluorescence mode showing nucleus staining with DAPI (blue, $\lambda_{ex}/\lambda_{em}$ = 405/450 nm, column a), fluorescein-labelled oxidized carbon nanoparticles (green, $\lambda_{ex}/\lambda_{em}$ = 488/510 nm, column b), endosome staining with EEA1 antibody (red, $\lambda_{ex}/\lambda_{em}$ = 555/561 nm, column c), and merged fluorescent signals (column d). White arrowhead indicated localization of OCNs and endosomes.

HepG2 cells were treated with 30 µg/ml of oxidized carbon nanoparticles at 37 °C under 5% CO_2 for 2 h. Then, the cells were fixed and incubated with EEA1 antibody. **Figure 3.14** showed fluorescent signals of various dye. Column a-d show nucleus, fluorescein-labelled OCNs, endosome and merge fluorescent signals. Row 1-4 display untreated cells, the cells that were treated with GOShs, OCTs and OCSs, respectively. The results in **Figure 3.14** revealed signals of all three shaped OCNs co-localized with endosome signals. Hence, OCSs, OCTs and GOShs were internalized into the cells through endosome.

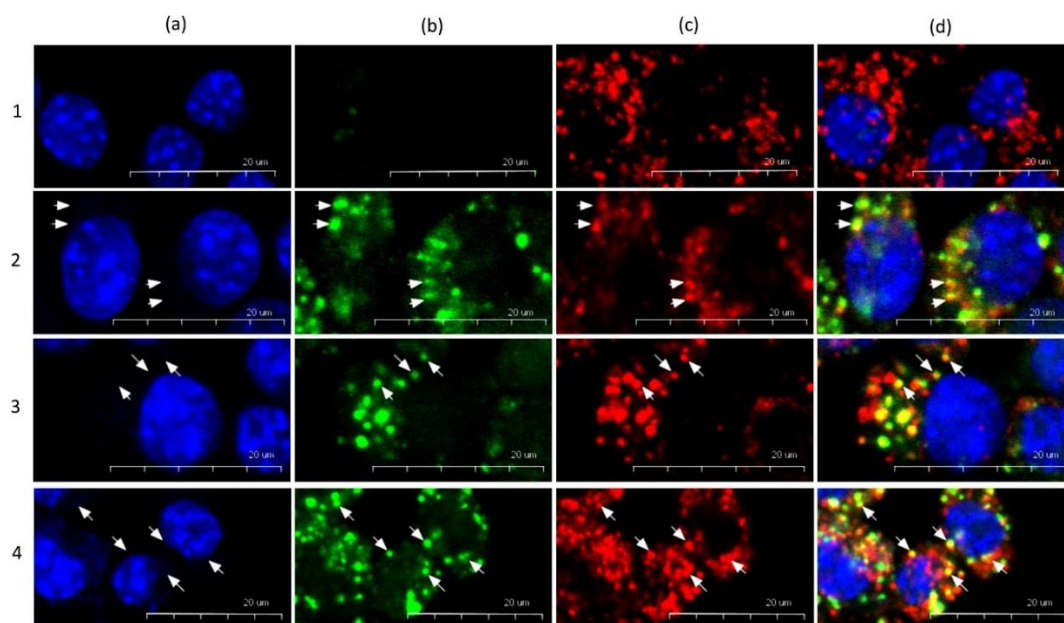### 3.2.3.2 Co-localization between oxidized carbon nanoparticles and lysosome in HepG2
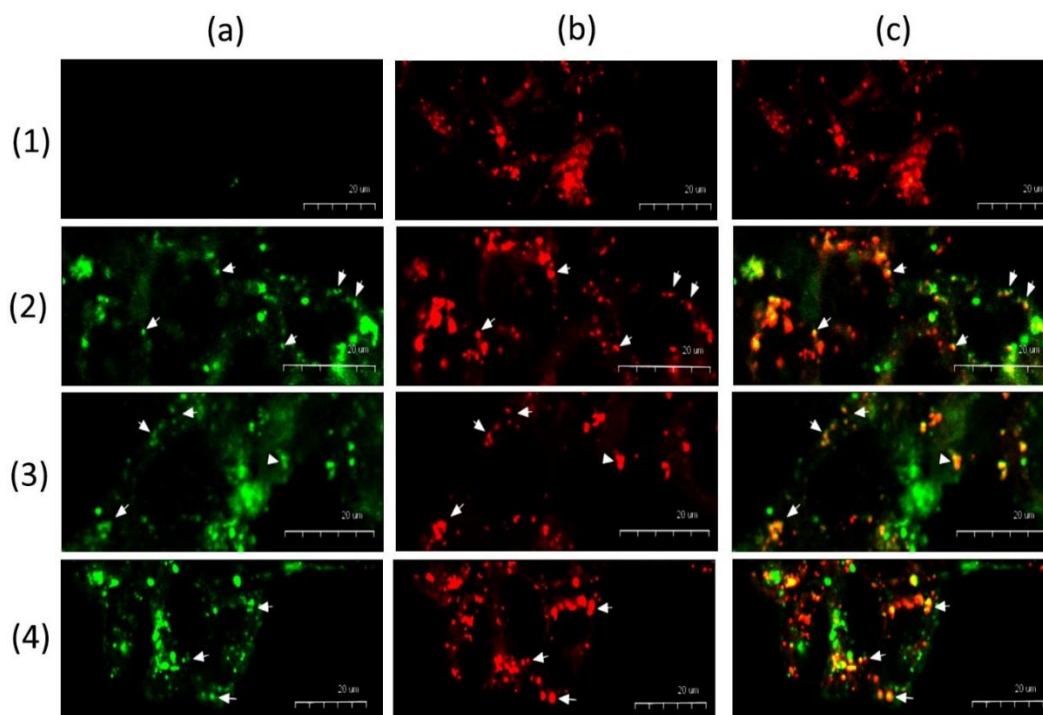
Figure 3.15: Intracellular trafficking of fluorescein-labelled oxidized carbon nanoparticles and lysosome in HepG2 cells: Cells incubated with no particles (row 1), GOShs$_{Flu}$ (row 2), OCTs$_{Flu}$ (row 3) and OCSs$_{Flu}$ (row 4). Image in the fluorescence mode showing fluorescein-labelled oxidized carbon nanoparticles (green, $\lambda_{ex}/\lambda_{em}$ = 497/519 nm, column a), lysotracker (red, $\lambda_{ex}/\lambda_{em}$ = 650/668 nm, column b), and merged fluorescent signals (column c). White arrowhead indicated co-localization in lysosome. White arrowheads indicated localization of OCNs and lysosomes.

HepG2 cells were incubated with oxidized carbon nanoparticles which their working concentration was controlled at 30 µg/ml. After that, the cells were incubated with lysotracker and fixed. Finally, the cells observed under CLSFM. **Figure 3.15** display fluorescent signals from fluorescein-labelled oxidized carbon nanoparticles (column a) lysotracker (column b) and merged fluorescent signals (column c). Row 1-4 display untreated cells, the cells that were treated with GOShs, OCTs and OCSs, respectively.

Signals of all three shaped OCNs co-localized with lysosome signals (column c). Thus, three shapes of oxidized carbon nanoparticles were trafficked through lysosomes.

3.2.3.3 Co-localization between oxidized carbon nanoparticles and endoplasmic reticulum and golgi apparatus in HepG2
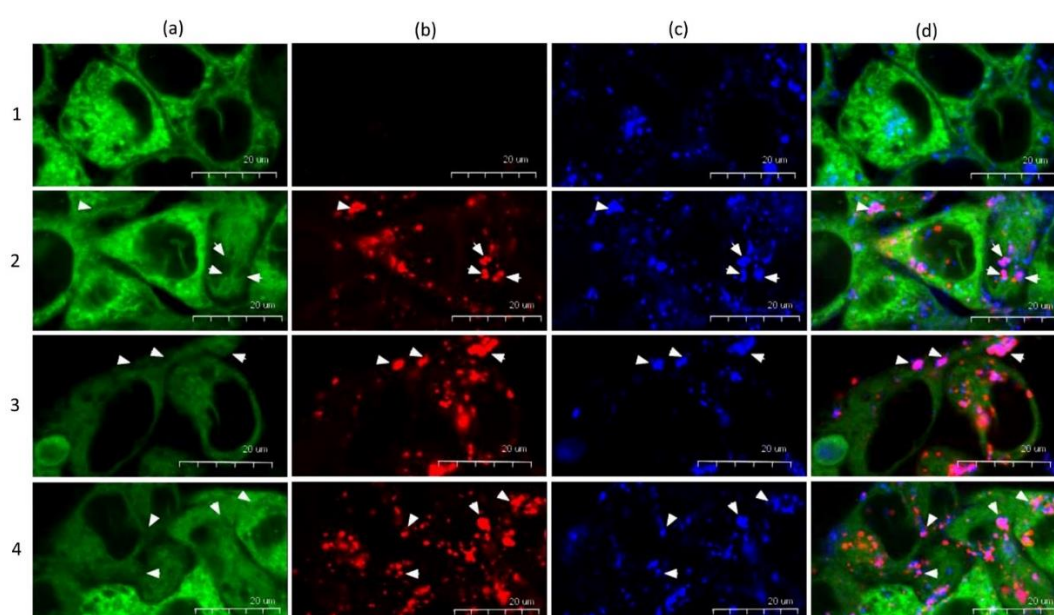
Figure 3.16: Intracellular trafficking of TAMRA-labelled oxidized carbon nanoparticles endoplasmic reticulum and golgi apparatus in HepG2 cells: Cells incubated with no particels (row 1), GOShs$_{TAMRA}$ (row 2), OCTs$_{TAMRA}$ (row 3) and OCSs$_{TAMRA}$ (row 4). Image in the fluorescence mode showing ER staning by CellLight® ER-GFP (green, $\lambda_{ex}/\lambda_{em}$ = 488/510 nm, column a), TAMRA-labelled oxidized carbon nanoparticles (red, $\lambda_{ex}/\lambda_{em}$ = 559/580 nm, column b), golgi apparatus staining by Alexa Fluor 647 conjugated lectin GS-II (blue, $\lambda_{ex}/\lambda_{em}$ = 650/668 nm, column c), and merged fluorescent signals (column d). White arrowhead indicated localization of OCNs and golgi apparatus.

HepG2 cells were incubated with 30 µg/ml of oxidized carbon nanoparticles. Then, the cells were incubated with ER-tracker and AF647-conjugated with lectin GS-II. After that, the cells were wash 2 times with PBS and observed with CLSFM immediately. **Figure 3.16** exhibited endoplasmic reticulum staining (column a), TAMRA-labelled oxidized carbon nanoparticles (column b), golgi apparatus (column c) and merged fluorescent signals (column d). Row 1-4 display untreated cells, the cells that were treated with GOShs, OCTs and OCSs, respectively. Signals of all three shaped oxidized carbon nanoparticles co-localized in golgi apparatus signals (column d) and did not in ER. Hence, three shapes of oxidized carbon nanoparticles were trafficked through golgi apparatus and were not in endoplasmic reticulum.

Table 3.5: Co-localization of three shapes of oxidized carbon nanoparticles and cellular compartments
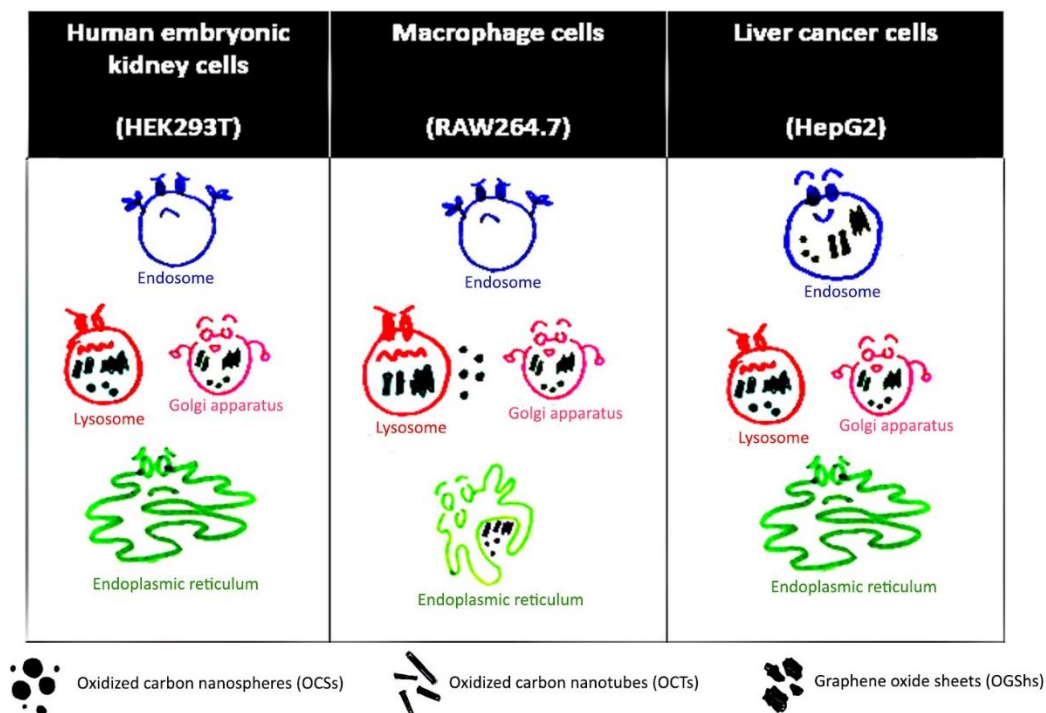
In **Table 3.5**, the results were concluded OCSs, OCTs and GOShs were not localized with endosome in HEK293T and RAW264.7 cells. Generally, cell membranes, that were composed of lipids, had region of lipid-ordered phase (L_o), and lipid-disordered phase (L_d), as shown in **Figure 3.17**. L_d had a loose packing of lipid and less rigid nature. In addition, oxidized carbon nanoparticles that had the potential associated with region of L_d phase and induced pore on lipid membranes [15, 23]. Hence, oxidzied carbon nanoparticles were internalized into the cells through association with region of L_d phase and induced pore on the cell membranes. In case of HepG2 , cancer cells had cholesterol enrichment in cell membrane which increased rigidity of lipid membrane (**Figure 3.17**) [58, 59]. Thus, the three shapes of OCNs, that prefer to associate with L_d phase, were internalized into the cells through endocytosis and found in HepG2's endosome.

Lysosome is the site of degradation for extracellular and intracellular substances. OCSs, OCTs and GOShs also were concluded that localized with lysosome

in HEK293T and HepG2 cells. These cells used lysosome for degradation OCNs and shuttled to the outside of the cells. In case of RAW264.7, only OCSs showed lysosomal trapping. Golgi apparatus were used for packing things into secretory vesicle or presenting on the cells membranes (**Figure 1.1**). Therefore, golgi apparatus were used for secretion of cell products, including the three shapes of OCNs. In addition, OCSs, OCTs and GOShs were localized with endoplasmic reticulum in RAW264.7 cells, which RAW264.7 is immune cells. Thus, endoplasmic reticulum in RAW264.7 was used for activation of immune system and found three shapes of OCNs in its [60].
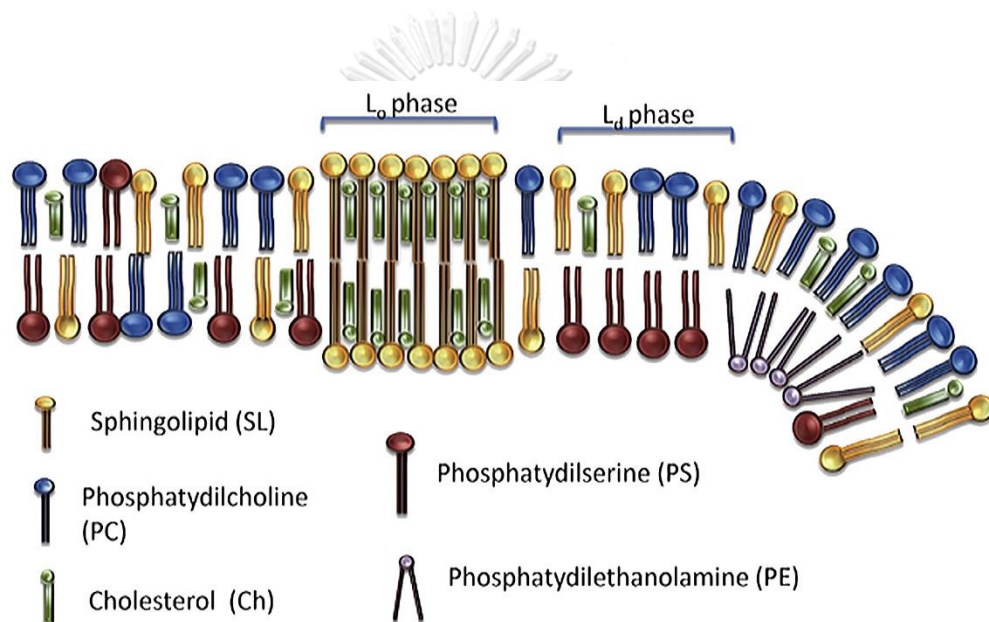
Figure 3.17: Schematic representation of a cellular membrane depicting a selection of phospholipids as they appear in a bilayer; L_o represented lipid-ordered phase, L_d represented lipid-disordered phase.

3.3 Comparison of cellular uptake between three shapes of oxidized carbon nanoparticles
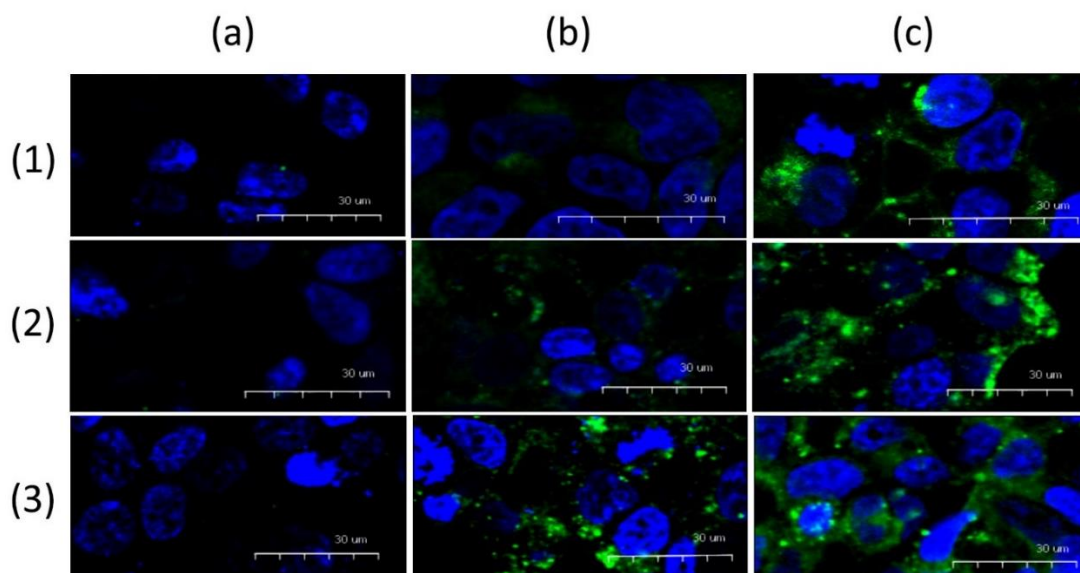
Figure 3 18: Comparison of cellular uptake between OCSs, OCTs and GOShs. CLSFM images of HEK293T cells after being incubated with GOShs (row 1), OCTs (row 2) and OCSs (row3) for 2h (column a), 4h (column b) and 6h (column c). Image in the fluorescence mode showing nucleus staining (blue, $\lambda_{ex}/\lambda_{em}$ = 405/450 nm) and fluorescein-labelled oxidized carbon nanoparticles (green, $\lambda_{ex}/\lambda_{em}$ = 497/519 nm).

HEK293T cells were treated with 10 µg/ml of oxidized carbon nanoparticles as working concentration at 37 °C under 5% CO_2 for 2h (column a), 4h (column b) and 6h (column c). After finish incubation, the cells were fixed and stained nucleus. In **Figure 3.17**, row 1-3 respectively display the cells that treated with GOShs, OCTs and OCSs. OCSs had intensity of signal was the highest, OCTs had moderate signals and GOShs had the lowest signals. Signals of OCSs in RAW264.7 cells were more than signals of OCTs and GOShs (**Figure 3.8**). Signals of three shaped OCNs in HepG2 cells were not different (**Figure 3.14**). Thus, OCSs had capable of cellular internalization more than OCTs, which was moderate, and GOShs, was lowest.

CHAPTER IV

CONCLUSION

In this research, I have prepared three shapes of oxidized carbon nanoparticles (OCNs), oxidized carbon nanospheres (OCSs), oxidized carbon nanotubes (OCTs) and graphene oxide sheets (GOShs). Intracellular trafficking pathway in human embryonic kidney cells (HEK293T), mouse macrophage cells (RAW264.7) and human liver cancer cells (HepG2) of the three shapes were investigated. Three shapes of OCNs were not internalized into HEK293T cells *via* endosome. OCSs, OCTs and GOShs were found in lysosomes and golgi apparatus and not in endoplasmic reticulum (ER). OCSs, OCTs and GOShs were internalized into RAW264.7 cells *via* endosome. OCTs and GOShs were found in lysosomes and OCSs were not found. Three shapes of OCNs were found in ER and golgi apparatus. Three shapes of OCNs had trafficking pathway that involved with exocytic pathway. OCS, OCTs and GOShs were found in ER and golgi apparatus. OCSs, OCTs and GOShs were internalized into HepG2 cells *via* endosomes. Three shapes of OCNs were found in lysosomes and golgi apparatus and not in ER. Comparison of cellular internalization between shape of OCNs showed OCSs was the fastest cellular internalization, OCTs was moderate and GOShs was the slowest cellular internalizatio

REFERENCES

1. Dugani, C.B. and Klip, A., Glucose transporter 4: cycling, compartments and controversies. Third in the Cycles Review Series 6(12) (2005): 1137-1142.

2. Schotman, H. and Rabouille, C., *The Exocytic Pathway and Development*, in *Trafficking Inside Cells: Pathways, Mechanisms and Regulation*. 2009, Springer New York: New York, NY. p. 419-438.

3. Janka, G.E., Familial and acquired hemophagocytic lymphohistiocytosis. European journal of pediatrics 166(2) (2007): 95-109.

4. Tang, Y., Olufemi, L., Wang, M.-T., and Nie, D., Role of Rho GTPases in breast cancer. Frontiers in bioscience: a journal and virtual library 13 (2008): 759-776.

5. Wu, G., Yussman, M.G., Barrett, T.J., Hahn, H.S., Osinska, H., Hilliard, G.M., Wang, X., Toyokawa, T., Yatani, A., and Lynch, R.A., Increased myocardial Rab GTPase expression: a consequence and cause of cardiomyopathy. Circulation research 89(12) (2001): 1130-1137.

6. Lin Chua, C.E. and Tang, B.L., α-synuclein and Parkinson's disease: the first roadblock. Journal of cellular and molecular medicine 10(4) (2006): 828-837.

7. Osman, M. and Cerione, R.A., *Actin doesn't do the locomotion: secretion drives cell polarization*, in *Trafficking Inside Cells*. 2009, Springer. p. 388-404.

8. Donaldson, J. and Segev, N., *Regulation and coordination of intracellular trafficking: an overview*, in *Trafficking Inside Cells*. 2009, Springer. p. 329-341.

9. Ajima, K., Yudasaka, M., Murakami, T., Maigné, A., Shiba, K., and Iijima, S., Carbon Nanohorns as Anticancer Drug Carriers. Molecular Pharmaceutics 2(6) (2005): 475-480.

10. Sun, X., Liu, Z., Welsher, K., Robinson, J.T., Goodwin, A., Zaric, S., and Dai, H., Nano-graphene oxide for cellular imaging and drug delivery. Nano research 1(3) (2008): 203-212.

11.   Bottini, M., Rosato, N., and Bottini, N., PEG-modified carbon nanotubes in biomedicine: current status and challenges ahead. Biomacromolecules 12(10) (2011): 3381-3393.

12.   Kim, H., Namgung, R., Singha, K., Oh, I.-K., and Kim, W.J., Graphene oxide–polyethylenimine nanoconstruct as a gene delivery vector and bioimaging tool. Bioconjugate chemistry 22(12) (2011): 2558-2567.

13.   Liao, K.-H., Lin, Y.-S., Macosko, C.W., and Haynes, C.L., Cytotoxicity of graphene oxide and graphene in human erythrocytes and skin fibroblasts. ACS applied materials & interfaces 3(7) (2011): 2607-2615.

14.   Qi, X., Rui, Y., Fan, Y., Chen, H., Ma, N., and Wu, Z., Galactosylated chitosan-grafted multiwall carbon nanotubes for pH-dependent sustained release and hepatic tumor-targeted delivery of doxorubicin in vivo. Colloids and Surfaces B: Biointerfaces 133(Supplement C) (2015): 314-322.

15.   Seemork, J., Sansureerungsikul, T., Sathornsantikun, K., Sinthusake, T., Shigyou, K., Tree-Udom, T., Jiangchareon, B., Chiablaem, K., Lirdprapamongkol, K., Svasti, J., Hamada, T., Palaga, T., and Wanichwecharungruang, S., Penetration of Oxidized Carbon Nanospheres through Lipid Bilayer Membrane: Comparison to Graphene Oxide and Oxidized Carbon Nanotubes, and Effects of pH and Membrane Composition. ACS Applied Materials & Interfaces 8(36) (2016): 23549-23557.

16.   Arayachukeat, S., Palaga, T., and Wanichwecharungruang, S.P., Clusters of Carbon Nanospheres Derived from Graphene Oxide. ACS Applied Materials & Interfaces 4(12) (2012): 6808-6815.

17.   Li, H., Fan, X., and Chen, X., Near-infrared light activation of proteins inside living cells enabled by carbon nanotube-mediated intracellular delivery. ACS applied materials & interfaces 8(7) (2016): 4500-4507.

18.   Villa, C.H., Dao, T., Ahearn, I., Fehrenbacher, N., Casey, E., Rey, D.A., Korontsvit, T., Zakhaleva, V., Batt, C.A., Philips, M.R., and Scheinberg, D.A., Single-Walled Carbon Nanotubes Deliver Peptide Antigen into Dendritic Cells and Enhance IgG Responses to Tumor-Associated Antigens. ACS Nano 5(7) (2011): 5300-5311.

19. Ceballos-Alcantarilla, E., Abad-Somovilla, A., Agulló, C., Abad-Fuentes, A., and Mercader, J.V., Protein-Free Hapten-Carbon Nanotube Constructs Induce the Secondary Immune Response. <u>Bioconjugate chemistry</u> 28(6) (2017): 1630-1638.

20. Wang, Y., Li, Z., Weber, T.J., Hu, D., Lin, C.-T., Li, J., and Lin, Y., In Situ Live Cell Sensing of Multiple Nucleotides Exploiting DNA/RNA Aptamers and Graphene Oxide Nanosheets. <u>Analytical Chemistry</u> 85(14) (2013): 6775-6782.

21. Cifuentes-Rius, A., Boase, N.R.B., Font, I., Coronas, N., Ramos-Perez, V., Thurecht, K.J., and Borrós, S., In Vivo Fate of Carbon Nanotubes with Different Physicochemical Properties for Gene Delivery Applications. <u>ACS Applied Materials & Interfaces</u> 9(13) (2017): 11461-11471.

22. Guo, C., Al-Jamal, W.T., Toma, F.M., Bianco, A., Prato, M., Al-Jamal, K.T., and Kostarelos, K., Design of cationic multiwalled carbon nanotubes as efficient siRNA vectors for lung cancer xenograft eradication. <u>Bioconjugate chemistry</u> 26(7) (2015): 1370-1379.

23. Arayachukiat, S., Seemork, J., Pan-In, P., Amornwachirabodee, K., Sangphech, N., Sansureerungsikul, T., Sathornsantikun, K., Vilaivan, C., Shigyou, K., and Pienpinijtham, P., Bringing macromolecules into cells and evading endosomes by oxidized carbon nanoparticles. <u>Nano letters</u> 15(5) (2015): 3370-3376.

24. Conibear, E. and Tam, Y.Y.C., *The Endocytic Pathway*, in *Trafficking Inside Cells: Pathways, Mechanisms and Regulation*. 2009, Springer New York: New York, NY. p. 67-83.

25. Gruenberg, J., Griffiths, G., and Howell, K.E., Characterization of the early endosome and putative endocytic carrier vesicles in vivo and with an assay of vesicle fusion in vitro. <u>The Journal of Cell Biology</u> 108(4) (1989): 1301-1316.

26. Entchev, E.V. and González-Gaitán, M.A., Morphogen gradient formation and vesicular trafficking. <u>Traffic</u> 3(2) (2002): 98-109.

27. Mullock, B.M., Branch, W.J., Van Schaik, M., Gilbert, L.K., and Luzio, J.P., Reconstitution of an endosome-lysosome interaction in a cell-free system. <u>The Journal of cell biology</u> 108(6) (1989): 2093-2099.

28.   Wessling-Resnick, M. and Braell, W., The sorting and segregation mechanism of the endocytic pathway is functional in a cell-free system. <u>Journal of Biological Chemistry</u> 265(2) (1990): 690-699.

29.   Kirchhausen, T., Three ways to make a vesicle. <u>Nature Reviews Molecular Cell Biology</u> 1(3) (2000): 187.

30.   Springer, S., Spang, A., and Schekman, R., A primer on vesicle budding. <u>Cell</u> 97(2) (1999): 145-148.

31.   Hauri, H.-P. and Schweizer, A., The endoplasmic reticulum—Golgi intermediate compartment. <u>Current opinion in cell biology</u> 4(4) (1992): 600-608.

32.   Tokarev, A.A., Alfonso, A., and Segev, N., *Overview of intracellular compartments and trafficking pathways*, in *Trafficking Inside Cells*. 2009, Springer. p. 3-14.

33.   Meléndez, A. and Levine, B., Autophagy in C. elegans. <u>WormBook</u> 24 (2009): 1-26.

34.   Wang, C.-W. and Klionsky, D.J., The molecular mechanism of autophagy. <u>Molecular medicine</u> 9(3-4) (2003): 65.

35.   Cha, C., Shin, S.R., Annabi, N., Dokmeci, M.R., and Khademhosseini, A., Carbon-based nanomaterials: multifunctional materials for biomedical engineering. <u>ACS nano</u> 7(4) (2013): 2891-2897.

36.   Li, H., Fierens, K., Zhang, Z., Vanparijs, N., Schuijs, M.J., Van Steendam, K., Feiner Gracia, N.l., De Rycke, R., De Beer, T., and De Beuckelaer, A., Spontaneous protein adsorption on graphene oxide nanosheets allowing efficient intracellular vaccine protein delivery. <u>ACS applied materials & interfaces</u> 8(2) (2016): 1147-1155.

37.   Chatterjee, A. and Deopura, B., Carbon nanotubes and nanofibre: an overview. <u>Fibers and Polymers</u> 3(4) (2002): 134-139.

38.   Kam, N.W.S., O'Connell, M., Wisdom, J.A., and Dai, H., Carbon nanotubes as multifunctional biological transporters and near-infrared agents for selective cancer cell destruction. <u>Proceedings of the National Academy of Sciences of the United States of America</u> 102(33) (2005): 11600-11605.

39. Jin, H., Heller, D.A., Sharma, R., and Strano, M.S., Size-dependent cellular uptake and expulsion of single-walled carbon nanotubes: single particle tracking and a generic uptake model for nanoparticles. Acs Nano 3(1) (2009): 149-158.

40. Bhirde, A.A., Patel, V., Gavard, J., Zhang, G., Sousa, A.A., Masedunskas, A., Leapman, R.D., Weigert, R., Gutkind, J.S., and Rusling, J.F., Targeted killing of cancer cells in vivo and in vitro with EGF-directed carbon nanotube-based drug delivery. ACS nano 3(2) (2009): 307-316.

41. Prato, M., Kostarelos, K., and Bianco, A., Functionalized carbon nanotubes in drug design and discovery. Accounts of chemical research 41(1) (2007): 60-68.

42. Pierre, P., Turley, S.J., Gatti, E., Hull, M., Meltzer, J., Mirza, A., Inaba, K., Steinman, R.M., and Mellman, I., Developmental regulation of MHC class II transport in mouse dendritic cells. Nature 388(6644) (1997): 787.

43. Faria, P.C.B.d., Santos, L.I.d., Coelho, J.o.P., Ribeiro, H.B.c., Pimenta, M.A.a.o., Ladeira, L.O., Gomes, D.A., Furtado, C.A., and Gazzinelli, R.T., Oxidized multiwalled carbon nanotubes as antigen delivery system to promote superior CD8+ T cell response and protection against cancer. Nano letters 14(9) (2014): 5458-5470.

44. Zhou, F., Xing, D., Wu, B., Wu, S., Ou, Z., and Chen, W.R., New insights of transmembranal mechanism and subcellular localization of noncovalently modified single-walled carbon nanotubes. Nano letters 10(5) (2010): 1677-1681.

45. Porter, A.E., Gass, M., Muller, K., Skepper, J.N., Midgley, P.A., and Welland, M., Direct imaging of single-walled carbon nanotubes in cells. Nature nanotechnology 2(11) (2007): 713.

46. Sanchez, V.C., Jachak, A., Hurt, R.H., and Kane, A.B., Biological interactions of graphene-family nanomaterials: an interdisciplinary review. Chemical research in toxicology 25(1) (2011): 15-34.

47. Park, S., An, J., Jung, I., Piner, R.D., An, S.J., Li, X., Velamakanni, A., and Ruoff, R.S., Colloidal suspensions of highly reduced graphene oxide in a wide variety of organic solvents. Nano letters 9(4) (2009): 1593-1597.

48.   Linares, J., Matesanz, M.C.n., Vila, M., Feito, M.J., Gonçalves, G., Vallet-Regí, M., Marques, P.A., and Portolés, M.T., Endocytic mechanisms of graphene oxide nanosheets in osteoblasts, hepatocytes and macrophages. <u>ACS applied materials & interfaces</u> 6(16) (2014): 13697-13706.

49.   Vilaivan, T. and Srisuwannaket, C., Hybridization of pyrrolidinyl peptide nucleic acids and DNA: Selectivity, base-pairing specificity, and direction of binding. <u>Organic letters</u> 8(9) (2006): 1897-1900.

50.   Xiao, Y.-F., Wright, S.N., Wang, G.K., Morgan, J.P., and Leaf, A., Fatty acids suppress voltage-gated Na+ currents in HEK293t cells transfected with the α-subunit of the human cardiac Na+ channel. <u>Proceedings of the National Academy of Sciences</u> 95(5) (1998): 2680-2685.

51.   Xiao, Y.-F., Ke, Q., Chen, Y., Morgan, J.P., and Leaf, A., Inhibitory effect of n-3 fish oil fatty acids on cardiac Na+/Ca 2+ exchange currents in HEK293t cells. <u>Biochemical and biophysical research communications</u> 321(1) (2004): 116-123.

52.   Wang, V., Davis, D.A., Haque, M., Huang, L.E., and Yarchoan, R., Differential gene up-regulation by hypoxia-inducible factor-1α and hypoxia-inducible factor-2α in HEK293T cells. <u>Cancer research</u> 65(8) (2005): 3299-3306.

53.   Jiang, W., Reich Iii, C.F., and Pisetsky, D.S., Mechanisms of activation of the RAW264. 7 macrophage cell line by transfected mammalian DNA. <u>Cellular immunology</u> 229(1) (2004): 31-40.

54.   Hamilos, D.L., Antigen presenting cells. <u>Immunologic research</u> 8(2) (1989): 98-117.

55.   Jagannath, C., Lindsey, D.R., Dhandayuthapani, S., Xu, Y., Hunter Jr, R.L., and Eissa, N.T., Autophagy enhances the efficacy of BCG vaccine by increasing peptide presentation in mouse dendritic cells. <u>Nature Medicine</u> 15 (2009): 267.

56.   Shintani, T. and Klionsky, D.J., Autophagy in Health and Disease: A Double-Edged Sword. <u>Science (New York, N.Y.)</u> 306(5698) (2004): 990-995.

57.   Yoshii, S.R. and Mizushima, N., Monitoring and measuring autophagy. <u>International journal of molecular sciences</u> 18(9) (2017): 1865.

58.   Mollinedo, F. and Gajate, C., Lipid rafts as major platforms for signaling regulation in cancer. <u>Advances in biological regulation</u> 57 (2015): 130-146.

59.   Zalba, S. and ten Hagen, T.L., Cell membrane modulation as adjuvant in cancer therapy. <u>Cancer treatment reviews</u> 52 (2017): 48-57.

60.   Dustin, M.L., The Cellular Context of T Cell Signaling. <u>Immunity</u> 30(4) (2009): 482-492.

VITA

Mr. Banphot Jiangchareon was born on September 3, 1991 in Samutprakarn. Thailand. He received a Bachelor 's Degree of Science in Chemistry from King Mongkut 's University of Technology Thonburi in 2013. He was started Master degree in the Biotechnology Program, Faculty of Science, Chulalongkorn University under the advisor of Prof. Supason Wanichwecharungruang.

His address is 1117 Bandung Road, Talad, Phrapadang, Samutprakarn 10130, Phone number: 063-859-5601.